COLLOIDAL SYNTHESIS AND DOPING OF SEMICONDUCTOR NANOCRYSTALS

A THESIS SUBMITTED TO
THE GRADUATE SCHOOL OF ENGINEERING AND SCIENCE
OF BILKENT UNIVERSITY
IN PARTIAL FULFILLMENT OF THE REQUIREMENTS FOR
THE DEGREE OF
MASTER OF SCIENCE
IN
ELECTRICAL AND ELECTRONICS ENGINEERING

By
Mehmet Zafer Akgül
July, 2015

COLLOIDAL SYNTHESIS AND DOPING OF SEMICONDUCTOR NANOCRYSTALS

By Mehmet Zafer Akgül

July, 2015

We certify that we have read this thesis and that in our opinion it is fully adequate, in scope and in quality, as a thesis for the degree of Master of Science.

Assoc. Prof. Dr. Hilmi Volkan Demir(Advisor)

Assist. Prof. Dr. Yegan Erdem

Assoc. Prof. Dr. Hamza Kurt

Approved for the Graduate School of Engineering and Science:

Prof. Dr. Levent Onural
Director of the Graduate School

ABSTRACT

COLLOIDAL SYNTHESIS AND DOPING OF SEMICONDUCTOR NANOCRYSTALS

Mehmet Zafer Akgül
M.S. in Electrical and Electronics Engineering
Advisor: Assoc. Prof. Dr. Hilmi Volkan Demir
July, 2015

Colloidal semiconductor nanocrystals have drawn great interest for application areas in photonics and optoelectronics thanks to their superior optical properties including strong bandgap emission and tunability. Also, their suitability for solution-based processing has made them highly attractive for low-cost production of light-emitting diodes and lasers. Our objective in this thesis is to show the potential and versatility of semiconductor nanocrystals via colloidal synthesis and post-processing methods. The thesis work includes the synthesis of colloidal quantum dot and well structures and their post-doping and investigates their exciton decay dynamics. In this thesis a novel colloidal approach for the doping of zinc blende colloidal quantum wells was proposed and demonstrated for the first time. This new doping method uniquely relies on atomic layer deposition (ALD) process. Here we achieved the worlds first manganese-doped CdSe@CdS core@shell nanoplatelets using our technique of ALD-assisted doping. Also, we studied silver-doped CdTe quantum dots under different conditions. Our experimental work proved that the quantum yield enhancement of silver-doped CdTe quantum dots is a strong function of the nanocrystal size and doping concentration. Tuning the nanocrystal size and doping level, our aqueous core-only CdTe nanocrystals reached a record high photoluminescence quantum efficiency of 68%. For these quantum dots, various decay kinetics were proposed and the enhancement in the quantum yield was attributed to the trap state annihilation. The methods and results provided in this thesis contribute to the fundamental understanding of semiconductornanocrystals and pave the way for high-performance colloidal platforms and devices.

Keywords: Semiconductor nanocrystals, nanoplatelets, colloidal quantum dots, colloidal quantum wells, doping, colloidal atomic layer deposition (ALD), colloidal

ALD-assisted doping.

ÖZET

YARIİLETKEN NANOKRİSTALLERİN KOLOİDAL SENTEZİ VE KATIKLANMASI

Mehmet Zafer Akgül
Elektrik ve Elektronik Mühendisliği, Yüksek Lisans
Tez Danışmanı: Doç. Dr. Hilmi Volkan Demir
Temmuz, 2015

Yarıiletken koloidal nanokristaller güçlü bant kenarı ışımaları ve ayarlanabilirliği gibi üstün optik niteliklerinden ötürü fotonik ve optoelektronik uygulama alanları için büyük ilgi çekmektedir. Ayrıca, solüsyon tabanlı işleme yöntemlerine uygunlukları kuantum nanokristallerini ışır diyotların ve lazerlerin düşük maliyetli üretimi için oldukça çekici hale getirmiştir. Bizim bu tezdeki amacımız yarıiletken nanokristallerin potansiyelini ve çok yönlülüğünü koloidal sentez ve sentez sonrası işlemler aracılığıyla göstermektir. Mevcut tez koloit halindeki kuantum noktacıklarının ve kuantum kuyularının sentezini ve sentez sonrası iyileştirme işlemlerini içermektedir ve bu yapılardaki eksiton yıkım dinamiklerini incelemektedir. Bu tezde ilk defa sfalerit yapıdaki koloidal kuantum kuyularının katıklanması için yenilikçi bir koloidal metot sunulmuştur. Bu yeni katıklama metodu koloidal atomik katman kaplama (K-AKK) işlemine dayanmaktadır. Bu şekilde, kendi geliştirdiğimiz K-AKK destekli katıklama tekniğiyle dünyanın ilk mangan katıklanmış CdSe@CdS nanoplakalarını elde ettik. Ayrıca, tezde gümüş katıklanmış CdTe kuantum noktacıklarını hazırladık ve farklı koşullar altında inceledik. Deneysel sonuçlarımız gümüş katıklanmış kuantum noktacıklarındaki kuantum verimlilik artışının nanokristal boyutunun ve katıklanma seviyesinin güçlü bir fonksiyonu olduğunu kanıtlamıştır. Nanokristal boyutunun ve katıklama seviyesinin ayarlanmasyla, suda çözünebilen sadece çekirdek halindeki CdTe kuantum noktacıklarımız %68 rekor kuantum verimliliğe ulaşmıştır. Bu kuantum noktacıklar için, çeşitli yıkım kinetikleri öne sürülmüş ve kuantum verimlilikteki artış, kapan noktalarının etkisiz hale getirilmesiyle ilişkilendirilmiştir. Bu tezde sunulan metotlar ve sonuçlar yarıiletken nanokristaller hakkındaki temel anlayışımıza katkıda bulunmakta ve yüksek performanslı koloidal nanokristal tabanlı platformlar ve cihazlar için zemin hazırlamaktadır.

Anahtar sözcükler: Yarıiletken nanokristaller, nanoplakalar, koloidal kuantum noktacıklar, koloidal kuantum kuyuları, katıklama, koloidal atomik katman kaplama (K-AKK), K-AKK destekli katıklama.

Acknowledgement

First, I want to thank my academic supervisor Prof. Hilmi Volkan Demir for his thesis supervision, and my thesis committee members Prof. Yegan Erdem and Prof. Hamza Kurt for serving on my thesis defense committee.

I would also like to thank my officemates as they have made the office life and lab work much more enjoyable for me during the last three years of my life. Starting from the beginning, their positive attitude towards my presence gave me the opportunity to learn, experiment and occasionally succeed. For the sake of truth, I enjoyed each and every minute passed in the lab trying the new stuff. For this, I present my deepest gratitude to my dear officemates: Can Uran, Shahab Akhavan, Yusuf Keleştemur, Burak Güzeltürk, Talha Erdem, Zeliha Soran-Erdem, Aydan Yeltik, Ahmet Fatih Cihan, İbrahim Akcalı, Halil Akcalı, Berkay Bozok, Onur Erdem and Sadi Ayhan. I should also thank Dr. Evren Mutlugün, Dr. Pedro L. Hernandez-Martinez, Dr. Gökçe Küçükayan, Dr. Nihan Kosku Perkgöz, Dr. Rohat Melik, Dr. Urartu Ö. Ş. Şeker, Dr. Vijay Kumar Sharma, Dr. Manoj Sharma, Dr. Murat Olutaş, Dr. Savaş Delikanlı, Özgün Akyüz, and Emre Ünal for their friendly support during my MS degree. Also, I would like to express my thanks to the former and other group members Cüneyt Eroğlu, Togay Amirahmadov, and Somayeh Fardindoost.

Last, I want to present my gratitude to my family for their priceless support, which kept me going through all those years. Without their support and direction, it would be very hard to find my way.

I would also like to acknowledge the financial support I received from TUBITAK BIDEB 2210 Program.

Contents

List of Figures

List of Tables

Chapter 1

Introduction

1.1 Motivation

With the recent advancements in the physics and chemistry in the nanometer regime, colloidal synthesis has provided us with a new kind of materials called nanocrystals. The nanocrystals are very small crystallites formed by a few hundred to a few thousand of atoms. The typical dimensions are in nanometers and can be changed to modify the intrinsic properties of the bulk material, such as the band gap. This dependence of the intrinsic material properties on the physical dimensions is due to the quantum confinement effect and forms the basis of the nanocrystal research.

In a bulk semiconductor, an electron and a hole are attracted to each other by the electrostatic Coulomb interaction thanks to their opposite charges. In this interaction total energy is reduced and a bound electron-hole pair is formed, which is called exciton [1]. The exciton has a distinct radius for each material, which is described by the exciton Bohr radius for that semiconductor [2]. If the physical dimensions of a structure become comparable to the respective exciton Bohr radius, more energy is needed to confine the exciton tight within the structure, thus the total energy of the exciton increases with merely decreasing the physical

size. This change in exciton energy affects the optical and electronic properties and enables us to engineer the properties of nanocrystals [3].

Numerous ways have been found to exploit the quantum confinement effect to have materials with enhanced properties. First, this effect was applied to thin-film growth techniques such as molecular beam epitaxy (MBE) and metal organic chemical vapor deposition (MOCVD) to produce different sorts and combinations of quantum well structures. The application of this physical phenomenon to optoelectronics has led to a big quantum leap in the optoelectronics industry and brought us to an age in which the advanced optoelectronic devices such as high power laser diodes, quantum well photodiodes and modulators are achieved [4–7]. This enabled us to conduct new experiments which were not previously possible.

Yet the MBE and MOCVD systems are complex and expensive. Moreover, these systems offer limited production capability in terms of possible quantum structures and they require lattice-matched high-quality substrates for a successful single-crystal growth. Due to these limitations, other ways to exploit quantum confinement effect in devices have been investigated and the colloidal synthesis techniques have been found to be capable of producing quantum structures with high-quality, lower cost and in a simpler and controllable way. With the advance of the colloidal synthesis techniques, different routes to produce various kinds of nanocrystals have been discovered. The chemical conditions to produce nanocrystals with shape-anisotropy have been explored and this has been applied to form more complex quantum structures, including nanocubes [8–10], nanorods [11,12], tetrapods [13–16], nanobelts [17], nanodumbbells [18,19] and, as the last one, the nanoplatelets [20]. The list can be expanded by including the different combinations and compositions of the core/shell structures. This flexibility to form any kind of nanostructure by benefiting from the colloidal route makes nanocrystals a promising candidate for the advanced electronic/optoelectronic devices of the future.

To harness the full potential of the colloidal nanostructures, however, some post-processing techniques are needed to enhance the existing properties and/or

to introduce new functionalities. To exemplify, the quantum yield, emission blinking and Auger recombination rate are intrinsic properties of colloidal quantum dots and, sometimes, may not be suitable for the application in hand [21, 22]. To increase the quantum yield and possibly reduce the blinking, for example, a shell in a Type-I or quasi-Type-II configuration can be coated onto the core-only nanocrystals for the proper passivation of the nanocrystal surface [23, 24]. The Auger recombination problem can be overcome by the use of a quasi-Type-II shell on the core-only nanocrystals [25–28].

As another aspect of the post-processing methods, new functionalities can be added to the existing nanocrystals with the use of a suitable chemistry. As an example, cation/anion exchange reactions can be performed on nanocrystal substrates within a solvent to form doped, alloyed or core/shell nanostructures with the adjustment of the reaction conditions and the relative amount of the precursors [29–35].

The main aim of this thesis work is to demonstrate the potential and versatility of the colloidal nanostructures by some examples of the colloidal synthesis and post-processing methods to improve the quality of the nanocrystals and to add new functionalities. Via post-processing techniques the tools available to obtain the materials with the desired properties increase significantly. Owing to the diversity and efficiency of the available tools, the adaptation of the colloidal nanocrystals into the next generation devices will be much faster and will result in advanced, low-cost and energy-efficient optoelectronics.

1.2 Thesis Overview

The organization of the remaining of this thesis is as follows:

Chapter 2 presents background information about semiconductor nanocrystals, starting from a simple physical picture to introductory colloidal nanocrystal synthesis and discussion of applications.

Chapter 3 is devoted to the colloidal quantum rings, a novel quantum well heterostructure having CdS/CdSe@CdS core/crown@shell architecture developed in this thesis.

In Chapter 4, a facile silver-doping procedure for aqueous cadmium telluride quantum dots is presented and experimental data are provided.

In Chapter 5, we present the colloidal atomic layer deposition-assisted manganese doping study on CdSe@CdS core@shell colloidal quantum wells, proposed and demonstrated in this thesis work.

Chapter 6 summarizes the results and findings of this thesis and gives a future outlook on the thesis work.

Chapter 2

Scientific Background

2.1 Physics of Quantum Structures

Due to the limited number of constituent atoms, size effects are observed in nanocrystals. The most prominent one is the quantum confinement effect, which results from the quantization of the energy bands in semiconductor nanocrystals. When the size becomes comparable to the exciton Bohr radius (Eq. 2.1), the effective band gap of the nanocrystal increases.

$$r_B = \frac{4\pi\epsilon\hbar^2}{\mu_{eff}q^2}, \qquad \mu_{eff} = \left(\frac{1}{m_e} + \frac{1}{m_h}\right)^{-1} \tag{2.1}$$

In Eq. 2.1, ϵ is the permittivity, $\hbar$ is the reduced Planks constant, m_e is the effective electron mass, m_h is the effective hole mass, and q is the elementary electron charge.

The effective energy bandgap of a quantum structure can be expressed as:

$$E_g^{Eff} = E_g^{Bulk} + E_{QC,total} \tag{2.2}$$

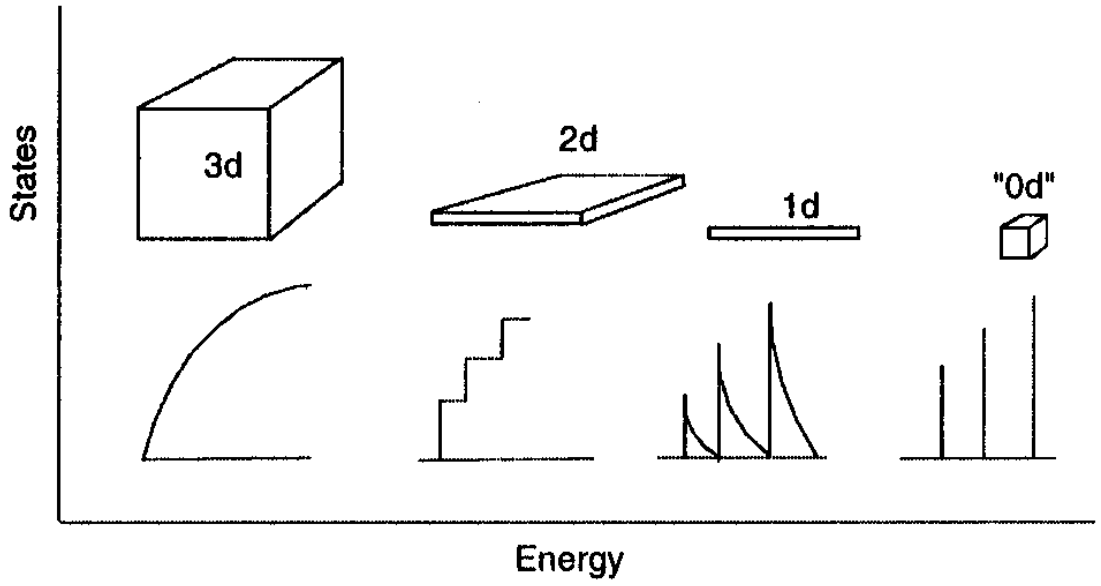

Figure 2.1: Energy vs. Density of States with respect to confinement type. Reprinted (adapted) with permission from A. P. Alivisatos [3]. Copyright 1996 American Chemical Society.

In Eq. 2.2, $E_{QC,total}$ denotes the quantum confinement energy due to the physically confined dimensions of the nanocrystal. The exact form of this energy depends on various complicated terms due to the complex nature of the physics of the nanocrystals, including material system, lattice system, and confinement type.

The confinement type is defined as the number of dimensions of a nanocrystal physically unconstrained. From this perspective, the simplest nanocrystals known as colloidal quantum dots can be identified as quasi-zero dimensional nanoparticles (quasi-0D, in short). These are point-like nanostructures confined in all three physical dimensions. The second largely utilized family is the colloidal quantum rods, or nanorods, and these are quasi-1D nanocrystals, elongated along one direction only. The latest one in the series is named colloidal quantum wells following the MOCVD/MBE thin film analogues and these belong to the quasi-2D nanocrystals family.

If the confinement type is different, the physical behavior of the optical transitions is different even for nanocrystals belonging to the same material system and

the same crystal structure with the same constituent atom types. This subtle effect results from the fact that the energy vs. density of states diagram is distinct for different confinement types (Figure 2.1) and this is reflected in the absorption and emission spectra [20, 36]. For the bulk case, the density of states follows a square-root relation with energy whereas it becomes staircase and spike-like for the quantum well and quantum dot case, respectively.

As the size of a piece of crystal gets smaller and smaller, its energy band structure is distorted due to the constructive and destructive interference of the wavefunctions of the charge carriers. This kind of interaction is well described by Schrdinger equation because of the quantum nature of the problem.

$$-\frac{\hbar^2}{2m_{c,i}}\nabla^2\psi_{c,i} + U\psi_{c,i} = i\hbar\frac{\partial^2}{\partial t^2}\psi_{c,i} \tag{2.3}$$

Here, $\psi_{c,i}$ is the carrier wavefunction, U is the potential and $m_{c,i}$ is the carrier effective mass in the crystal. Under time-independent conditions, this can be written as follows:

$$-\frac{\hbar^2}{2m_{c,i}}\nabla^2\psi_{c,i} + U\psi_{c,i} = E_{c,i}\psi_{c,i} \tag{2.4}$$

In Eq. 2.4, $E_{c,i}$ denotes the total energy of the carrier in the i^{th} energy level. The leftmost term in Eq. 2.4 gives the kinetic energy of the carrier while the middle term determines the potential energy of the carrier at the given position.

As a result of quantum confinement, the total energy of an electron in a finite crystal is different from that in an infinite crystal. We can understand this phenomenon easily by solving Schrdingers equation with some simplifying assumptions. First, we can assume that the potential is constant in a homogeneous material and for simplicity we can further assume that the potential energy within the material with the lowest conduction band level is zero. For the case at hand, the difference in the conduction band levels of the material and the surrounding medium is infinite. Thus,

$$U_{material} = 0, \quad U_{surrounding} \to \infty \tag{2.5}$$

$$-\frac{\hbar^2}{2m_{c,i}}\nabla^2\psi_{c,i} = E_{c,i}\psi_{c,i}$$

$$\nabla^2\psi_{c,i} = -k_{c,i}^2\psi_{c,i}, \quad \vec{k_{c,i}} = \vec{a_k}\frac{\sqrt{2m_{c,i}E_{c,i}}}{\hbar}$$

$$\psi_{c,i}(\vec{r}) = A_{c,i}e^{-i\vec{k_{c,i}}\cdot\vec{r}} + B_{c,i}e^{i\vec{k_{c,i}}\cdot\vec{r}} \tag{2.6}$$

$$\psi_{c,i}(\vec{r}) = C_{c,i}sin(\vec{k_{c,i}}\cdot\vec{r}) + D_{c,i}cos(\vec{k_{c,i}}\cdot\vec{r}) \tag{2.7}$$

Continuing from Eq. 2.7, we can derive E-k relation for the quasi-0D, quasi-1D and quasi-2D nanocrystals. For the quantum dot case, we can assume that it is a cube with a corner length of d (Figure 2.2). Thus, along a single axis, e.g., x-axis, we can write:

$$\psi_{c,i}(\vec{r} = 0) = 0 = C_{c,i}sin(0) + D_{c,i}cos(0)$$

$$D_{c,i} = 0$$

$$\psi_{c,i}(\vec{r} = d) = 0 = C_{c,i}sin(k_{x,n}d_x)$$

$$k_{x,n}d_x = n\pi \to k_{x,n} = \frac{n\pi}{d_x} \quad and \quad E_{QC,x} = \frac{\hbar^2 k_{x,n}^2}{2m_{c,i}}$$

$$E_{QC,n} = \frac{\hbar^2}{2m_{c,i}}\left(k_{x,n}^2 + k_{y,n}^2 + k_{z,n}^2\right) \tag{2.8}$$

When confined in all the three dimensions of space for the quantum dot case, the restriction on the wavevector is valid for all the three directions; thus, as a first order approximation, we can write $E_{QC,total} \sim 3E_{QC,x}$.

For the case of a nanorod (quasi-1D object) with a d-long square profile and a very long third dimension, we can easily see that the total confinement energy will be lower than that of the quantum dot case. Following the same reasoning above, we can see that $E_{QC,total} \sim 2E_{QC,x}$ as the long axis of the nanorods has no significant effect on the quantum confinement energy.

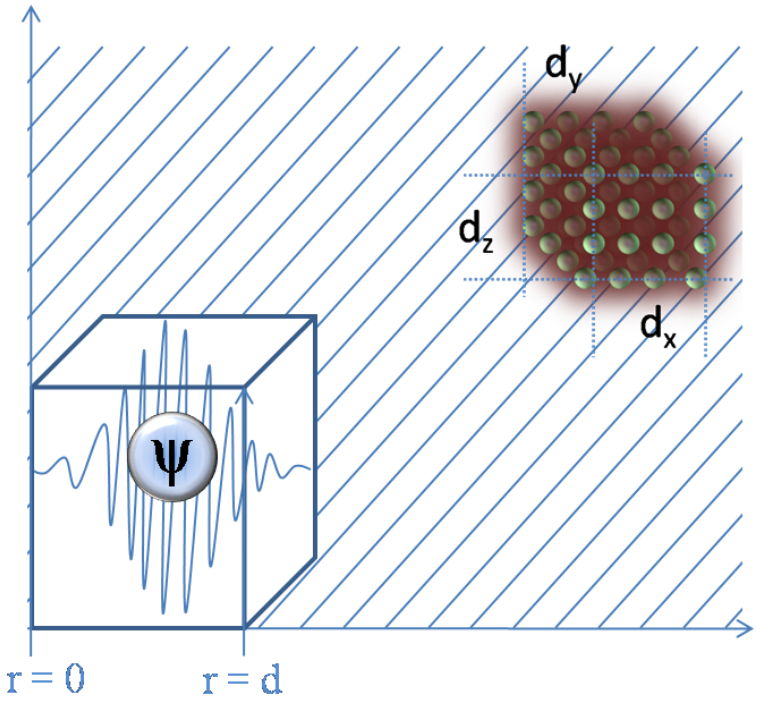

Figure 2.2: Schematic representation of the quantum box with infinite barriers problem (Inset: a 3D representation of a quasi-0D cubic quantum dot.

For the recently introduced member of the nanocrystal family, the quasi-2D nanoplatelets, the confinement energy decreases further due to the other two unconstrained dimensions, hence $E_{QC,total} \sim E_{QC,x}$ assuming that the nanoplatelets are confined in the x-direction. Thus, for the same length for the confined dimension(s), the relation between the resulting quantum confinement energies becomes $E_{QC,0D} > E_{QC,1D} > E_{QC,2D} > E_{QC,3D(bulk)} = 0$.

Although the explanation provided above oversimplifies the current picture, it gives insight for the optical behavior of the colloidal nanocrystals and enables us to interpret experimental data. To exemplify, for the case of CdSe materials system a widely used model semiconductor system the same peak emission wavelength can be achieved for nanocrystals with different confinement type. Both a CdSe quantum dot and a CdSe nanoplatelet can emit at 512 nm, although the former is a quasi-0D and the latter is a quasi-2D nanocrystal. From the approximate results obtained above, we can infer that the size of the CdSe quantum dot has to be larger than that of the confined dimension of the CdSe nanoplatelet to achieve

the same emission wavelength. Indeed, the diameter of the CdSe quantum dot is found to be 2.5 nm whereas the thickness of the CdSe nanoplatelet is around 1.4 nm [37, 38].

2.2 Colloidal Synthesis of Nanocrystals

In this part, some general information regarding the synthesis procedures used to produce colloidal nanocrystals will be presented to prepare the reader for the following chapters. The details of the synthesis and the post-processing methods utilized for each study will be provided in the respective chapter of this thesis.

Starting from the first demonstration of the quasi-0D colloidal quantum dots, the evolution and progress of the methods applied to the colloidal synthesis are tremendous within the past two decades. With the rapid development of the new techniques, the colloidal methods have become an inevitable choice for the synthesis of certain kind of nanostructures as there is no reliable and controllable alternative way for their production.

To understand the methods used in colloidal synthesis, we can group the nanocrystals into two basic categories and examine them accordingly. The first group consists of the nanocrystals that can be dispersed in solvents with a low polarity index such as hexane, octane and toluene and they are called nonpolar-soluble nanocrystals or nonpolar nanocrystals in short. The second group is the water-soluble/aqueous or polar nanocrystals and they can be dispersed in solvents with a high polarity index, including water and n-methyl formamide.

For the synthesis of nonpolar nanocrystals, there are two main routes. The first and the most widely used one is the hot-injection method. In this method, a host medium with a high boiling point is loaded into a flask with or without additional chemicals. After the flask reaches a certain temperature, a precursor solution, generally prepared under inert atmosphere (see Figure 2.3), is swiftly injected into the flask and the nucleation of nanocrystals occurs. After the nanocrystals reach

Figure 2.3: Glove box system to handle oxygen-sensitive chemicals.

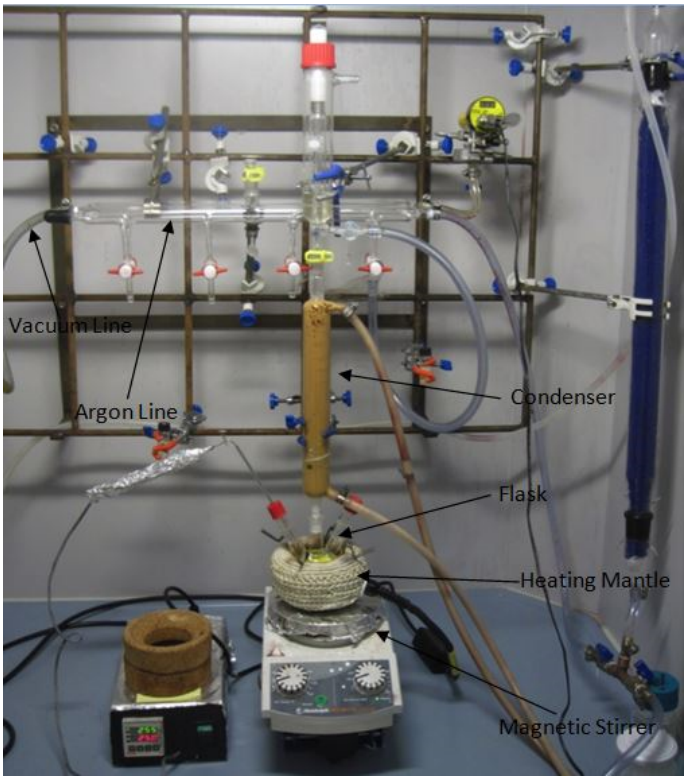

Figure 2.4: A typical setup for the synthesis of nonpolar quantum dots (from our laboratory at Bilkent UNAM).

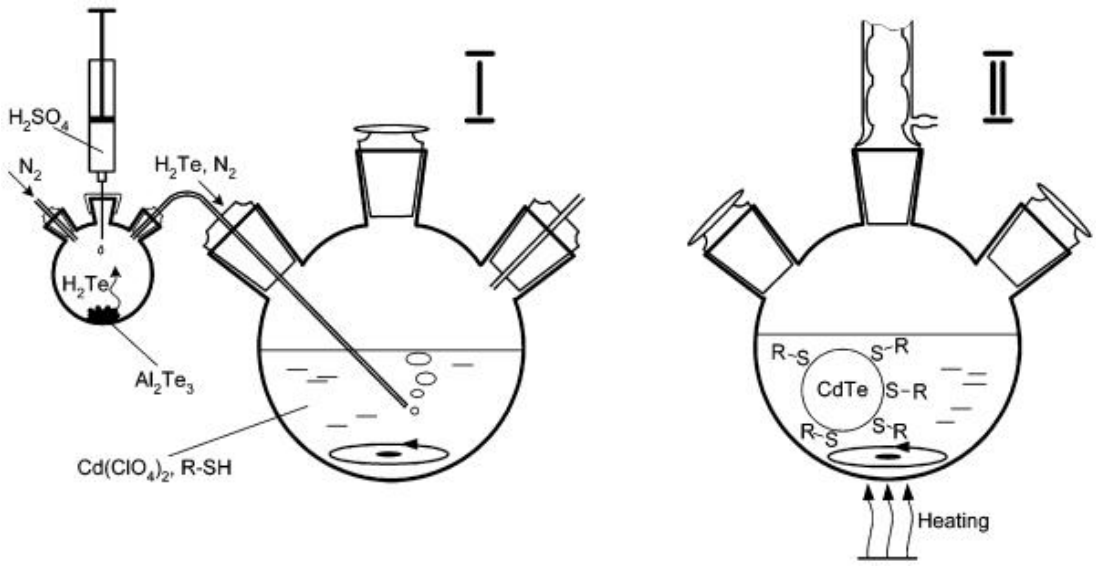

Figure 2.5: A representation for the typical equipment used for the synthesis of the aqueous CdTe QDs. Reprinted (adapted) with permission from N. Gaponik et al. [41] Copyright 2002 American Chemical Society.

the desired size/shape, the flask is cooled to room temperature and the resulting nanocrystals are purified with the addition of a non-solvent and centrifugation. In the second method called heat-up method, all of the ingredients are loaded into the flask before the synthesis begins. Then, the temperature of the flask is raised up in a controlled manner. During the heating the nucleation and growth of the nanocrystals occur. Then follow the cleaning steps to obtain a usable product. The most widely used ligands in the synthesis of the nonpolar nanocrystals are the carboxylic acids, phosphonic acids, amines and different combinations of them [12, 39, 40].

For visual assistance to the reader, a typical experimental setup for the synthesis of nonpolar quantum dots is given in Figure 2.4.

For the aqueous synthesis of nanocrystals, the most widely used technique is the aqueous heat-up method (Figure 2.5). For this type of synthesis, the cation precursor is dissolved in deionized water and a suitable ligand is added into the solution. The type of the ligand is chosen according to the desired functionalities and it is generally a mercaptan, such as thioglycolic acid and 3-mercaptopropionic

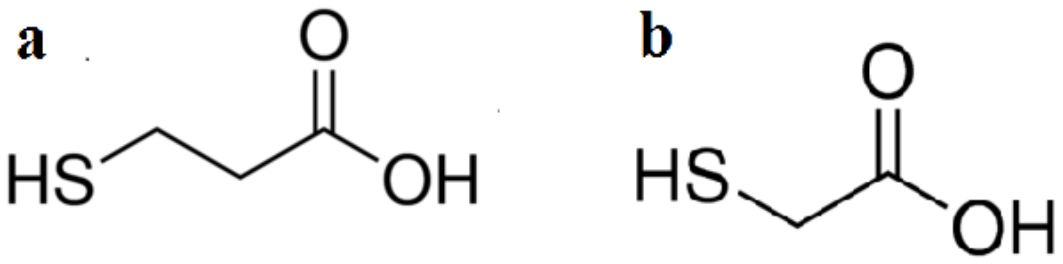

Figure 2.6: (a) 3-mercaptopropionic acid, (b) 2-thioglycolic acid.

acid (Figure 2.6) [42, 43].

Subsequently, the pH of the solution is brought to the required value with the drop-wise addition of an aqueous solution of a strong base, such as sodium hydroxide and potassium hydroxide. The final pH of the solution mainly depends on the identity of the ligand(s) used [41]. After the pH adjustment, the anions are introduced into the flask and the resulting solution is refluxed until the nanocrystals reach the desired size.

2.3 Colloidal Atomic Layer Deposition (c-ALD)

Colloidal atomic layer deposition technique is an ambient temperature method used for the shell coating of colloidal nanoparticles [44]. c-ALD offers a superior shell thickness control and gives an opportunity to deposit a shell on nanoplatelet substrates as the older methods, such as SILAR, failed to fulfill this task [39].

The procedure depends on the ability of Cd^{2+} and S^{2-} ions making nanoplatelets dispersible in polar media. At the first step, the colloids to be shell-coated is purified and dissolved in a nonpolar solvent, which is not mixable with the polar solvent to be utilized. For this purpose, the most commonly used polar and nonpolar solvents are formamide (FA)/n-methyl formamide (NFA) and hexane, respectively. FA and NFA have a special role in this process thanks to their high dielectric constant, which makes them perfect dispersants for the shell-coated nanocrystals. In the previous studies, it has been shown that the colloids

stay stable for longer time if they are dispersed in FA and kept in an air-tight glove box [45].

First, the nanocrystals dispersed in hexane are put into a falcon tube and 1 mL of NFA is added. At this point, two separate phases are observed and NFA phase is colorless, indicating the absence of nanocrystals. Then, ammonium sulfide is added and the mixture is stirred to ease the phase-transfer of the nanocrystals. After a few minutes, all the nanocrystals pass into the NFA phase and their color change, showing the successful coating of sulfur layer on the nanocrystal surface. The top hexane phase is then discarded and pure hexane is added. After a short stirring, the hexane phase is discarded again to remove the original ligands and the nanocrystals that failed to phase-transfer. Then, a mixture of toluene and acetonitrile is added to reduce the solubility of the sulfur-coated nanocrystals. Centrifugation is utilized to collect the precipitated colloids and later they are dispersed in pure NFA. The purification step is repeated once more to ensure the complete removal of sulfur precursor, which otherwise causes over-coating of the sample at later stages.

For deposition of the cationic layer, the acetate salt of cadmium is used as it is commercially available and readily soluble in NFA. For this step, a cadmium precursor stock solution is prepared by dissolving cadmium acetate in NFA. Then, the cadmium precursor is added to the NFA dispersion of the purified and sulfur-coated nanocrystals. Another color change is observed at this stage, which indicates the reduction of quantum confinement energy due to the increasing size of the nanocrystals. Then, the purification step is repeated twice to remove excess cadmium from the solution. As it is coated with a cadmium layer now, the nanocrystals can be reacted with sulfur precursor again, enabling the repetition of the whole cycle to deposit one more monolayer of shell.

A process flow diagram is provided in Figure 2.7. Here, didodecyldimethyl ammonium bromide (DDAB) is used for phase transfer of NPLs from FA to toluene to purify the NPL dispersion. In our study, we did not utilize DDAB as we did not need nonpolar nanocrystals. Instead, we precipitated NPLs with toluene-acetonitrile mixture for purification. In Figure 2.7, the red-shifting absorption and

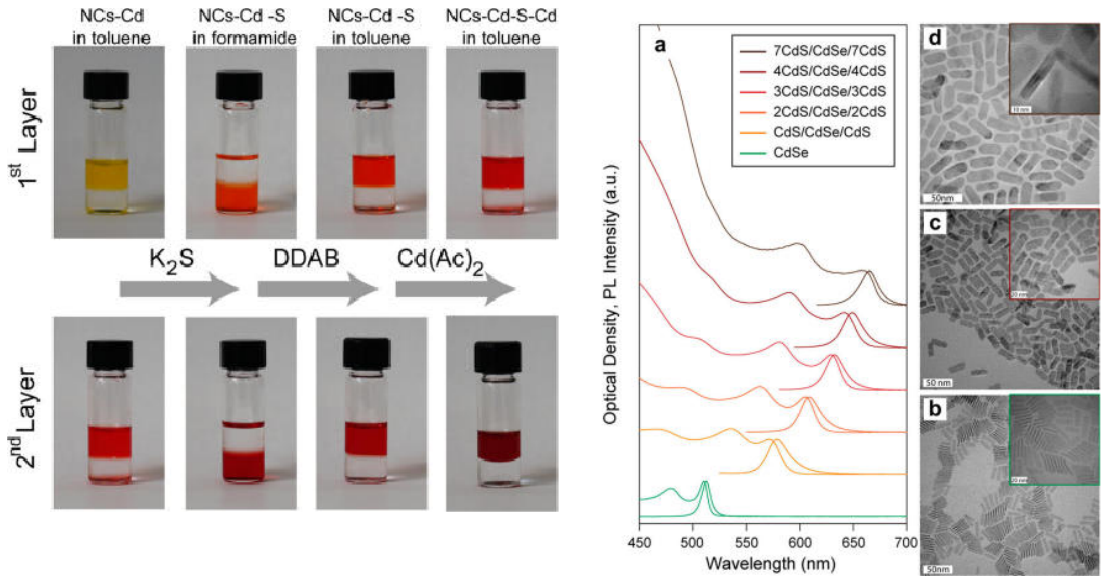

Figure 2.7: (Left) c-ALD process and (Right) the optical and structural characterization of the resulting core@shell nanoplatelets. Reprinted (adapted) with permission from S. Ithurria and D. V. Talapin [44]. Copyright 2012 American Chemical Society.

photoluminescence peaks, given in the right, clearly demonstrate the narrowing of the effective bandgap due to the increasing thickness of NPLs.

2.4 Application Areas of Colloidal Nanocrystals

In nanocrystals, the energy levels are quantized owing to the quantum confinement effect. As a result, the luminescence from nanocrystals can be adjusted over a broad range by changing their size (see Figure 2.8). Moreover, the colloidal synthesis allows the production of core/shell, alloyed and gradient nanostructures, thus providing alternative ways to adjust the optical bandgap, electronic configuration and surface passivation of the nanocrystals. The whole visible spectrum can be covered by nanocrystals of one type of material family. This capability of nanocrystals makes them valuable as active media for the optoelectronic applications, including light-emitting diodes, lasers, solar cells and light detectors [46–49].

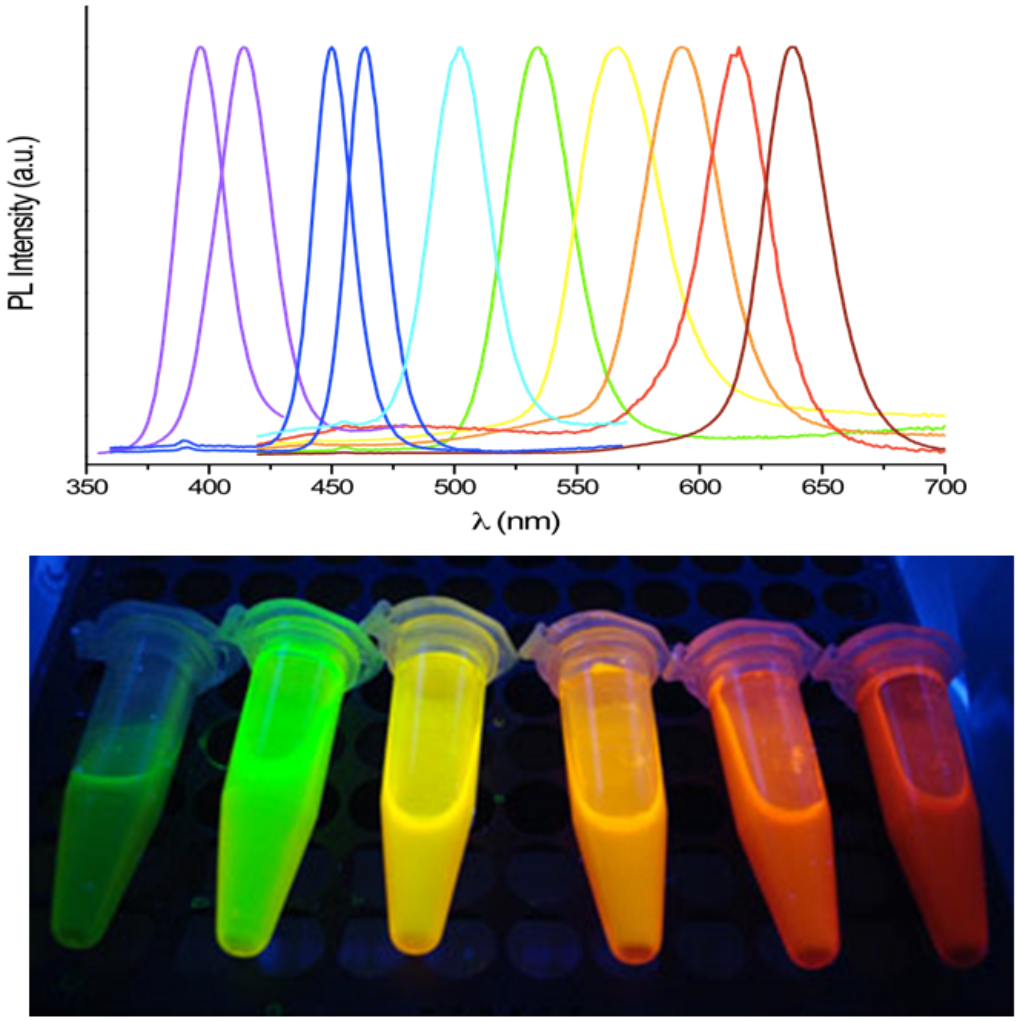

Figure 2.8: Upper: PL spectra of the CdZnSeS QDs of II-VI family. Lower: CdSe quantum dots with varying radii emitting in the green-red interval under UV excitation.

Chapter 3

A New Colloidal Quantum Well Heterostructure: Quantum Rings

3.1 Introduction

Starting from their first demonstration, colloidal semiconductor nanocrystals have attracted significant attention thanks to their promising properties and potential applications. The nanocrystal research initiated with simple quasi zero-dimensional (quasi-0D) structures namely solution-processed quantum dots has continued its progress with more anisotropic structures, such as nanorods, nanocubes, nanodumbbells and nanotetrapods [18, 19, 50–54]. Recently, it has been shown that it is also possible to synthesize highly anisotropic atomically-flat quasi-2D structures, commonly dubbed nanoplatelets (NPLs), with favorable and unique optical properties as compared to their quasi-0D and quasi-1D counterparts [55]. In addition, with the growth of a suitable shell, the physical and electronic properties of the core-only NPLs can be modified, which can be exploited for various device applications. For example, their quantum yield, photo-stability and fluorescence emission blinking can be significantly improved with precise control of the shell deposition turning them into highly advantageous candidates for LEDs, optical gain media and biological imaging [23, 56–62]. Very

recently, the first heterostructures of NPLs, core/shell and core/crown have also been demonstrated [37, 44, 63].

Also, NPLs with Type-I and Type-II electronic structures have been reported and in these novel heterostructures, the shell and crown layers can be grown on the seed NPLs with precise thickness control [63, 64]. Currently, these NPL heterostructures have been under intense research owing to their robust control of the shell and crown growth, and exceptional optical features, including high quantum yield (∼80%) and reduced fluorescence emission blinking [65]. Although different variations of these structures have been reported, these are confined to either only core/crown or only core/shell structures to date [37, 63]. The growth of NPL heterostructures containing both crown and shell components together has not been shown. This is significantly important, since it would introduce a new method for bandgap engineering in NPLs, which can be exploited for various device architectures.

Here, we report the colloidal synthesis and optical properties of a new family of NPLs, quantum rings (QRings), having a CdS/CdSe@CdS core/crown@shell heterostructure. These atomically-flat colloidal quasi-2D heterostructures were formed by embedding a CdSe crown layer between the 4 ML CdS core and the CdS shell with varying thickness. First, 4 ML CdS NPLs were synthesized and a CdSe crown was grown laterally around the 4 ML CdS NPLs using core-seeded method. Afterwards, the core/crown NPLs were coated with a CdS shell via colloidal atomic layer deposition (c-ALD) on CdS/CdSe core/crown NPLs emitting at 513 nm. We studied the resulting excitonic and optical properties of these QRings by varying the number of the CdS layers deposited on the CdS/CdSe NPLs through the absorption, photoluminescence (PL) and time-resolved fluorescence (TRF) measurements. This part is partially or fully taken from our journal publication article (M. Z. Akgul et al.), which is currently under submission.

3.2 Experimental Methods

3.2.1 Chemicals

Cadmium nitrate tetrahydrate ($Cd(NO_3)_2 \cdot 4H_2O$), sodium myristate, technical grade 1-octadecene (ODE), selenium (Se), sulfur (S), cadmium acetate dihydrate ($Cd(OAc)_2 \cdot 2H_2O$), ammonium sulfide ($S(NH_4)_2$, 40-48% wt. solution in H_2O), N-methyl formamide (NFA) and technical grade oleic acid (OA) were purchased from Sigma-Aldrich. Methanol, ethanol, acetone, toluene, acetonitrile, and hexane were purchased from Merck Millipore.

3.2.2 Preparation of cadmium myristate

Cadmium myristate was produced using the procedure given in the literature [63]. First, 1.23 g of ($Cd(NO_3)_2 \cdot 4H_2O$) and 3.13 g of sodium myristate were added in 40 mL and 250 mL of methanol in seperate beakers, and magnetically stirred until the complete dissolution. Then, ($Cd(NO_3)_2 \cdot 4H_2O$) solution was added into the vigorously stirred sodium myristate solution and was left stirring around 1 h untill the formation of a whitish precipitate. The precipitate was collected using centrifugation and the supernatant was discarded. Then, the precipitate was dissolved in methanol and centrifuged again. This purification stepl was repeated three times. Then the whitish precipitate was kept under vacuum overnight to remove the solvents.

3.2.3 Synthesis of 4 ML CdS NPLs

4 ML thick CdS NPLs were produced by a modified recipe found in the literature [66]. First, 217 mg of ($Cd(OAc)_2 \cdot 2H_2O$), 2 mL of 0.1 M S in ODE, 0.36 mL of OA, and 10 mL of ODE were put into a three-neck flask. Under argon protection, the temperature of the mixture was increased to 250°C within 20 min and kept

at this temperature for 2 min. Then, the flask was quickly cooled down to room temperature. CdS NPLs were seperated out of the mixture with the addition of acetone and centrifugation, and then dispersed in hexane for further use.

3.2.4 Preparation of anisotropic growth mixture

The precursor for CdSe crown growth was prepared using a slightly modified recipe found in the literature [63]. 480 mg of ($Cd(OAc)_2 \cdot 2H_2O$), 340 μL of OA, and 2 mL of ODE were put into a three-neck flask. At room temperature, it was sonicated for half an hour. Under air, the temperature of the mixture was increased to 160°C with continuous stirring and frequent sonication until the formation of a homogenous gel. 3 mL of 0.1 M ODE-Se solution was prepared in a N_2-filled glove box and added into the cadmium precursor with stirring.

3.2.5 CdSe crown growth

15 mL of ODE and 4 ML CdS NPLs dispersed in hexane were loaded into a three-neck flask. The temperature of the mixture was elevated to and kept at 80°C under vacuum about 1 h for the removal of the volatile hexane. Then, the flask was heated to 255°C under argon protection. At 255°C, the precursor mixture for CdSe crown growth was injected at a rate of 3 mL/h. After the injection, the flask was quickly cooled down to room temperature. CdS/CdSe core/crown NPLs were seperated out of the reaction mixture with the addition acetone and centrifugation, and then dispersed in hexane for further use.

3.2.6 CdS shell growth

CdS shell growth was performed with a similar procedure found in the literature [44]. 1 mL of NFA and 4 ML CdS/CdSe core/crown NPLs dispersed in 1 mL of hexane were added into a tube. To this two-phase mixture, aqueous ammonium

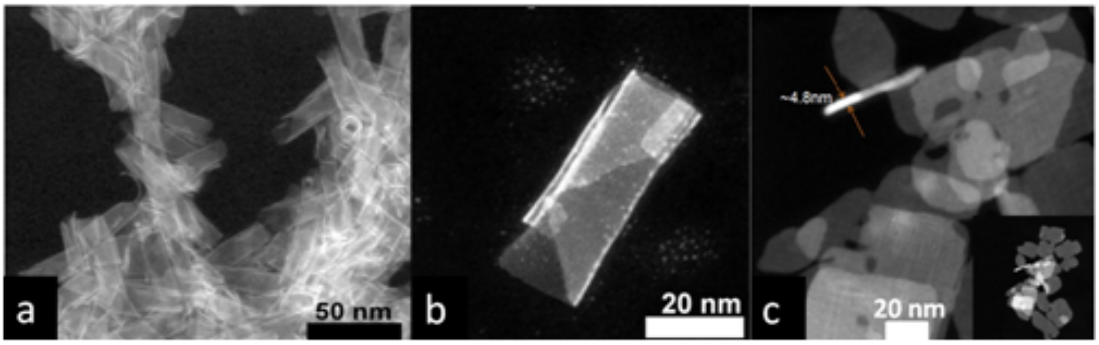

Figure 3.1: TEM images of (a) CdS core NPLs, (b) a CdS/CdSe core/crown NPL and (c) 4SCd QRings.

sulfide solution was added. After stirring, the NPLs were phase-transferred from hexane to NFA. Then, the hexane phase was discarded. NPLs were precipitated via the addition of toluene/acetonitrile mixture and centrifugation. The resulting NPL precipitate was dispersed in NFA and the cleaning step was repeated twice more to ensure the removal of excess precursor molecules. To complete one CdS shell deposition cycle, cadmium acetate precursor (dissolved in NFA) was added to NPL solution in NFA. Then, NPLs were cleaned using the same procedure given above. The shell deposition cycle was repeated 4 times to obtain the final 12 ML-thick QRings (Sample 4SCd).

3.3 Results and Discussion

In this part, we report the synthesis and optical properties of core/crown@shell type CdS/CdSe@CdS QRings. 4 ML-thick CdS cores were synthesized according to the recipe found in the literature with slight modifications [66]. Length of the CdS NPL seeds along the direction they rolled up was determined to be 40 nm 6 nm using high-angle annular dark-field transmission electron microscopy (HAADF-TEM) images (Figure 3.1).

As the CdS NPLs tend to stack and fold, it is difficult to extract the exact size distribution data from the TEM images. The light-hole and heavy-hole transitions of the 4 ML CdS NPLs are close to each other and form a relatively-broad peak

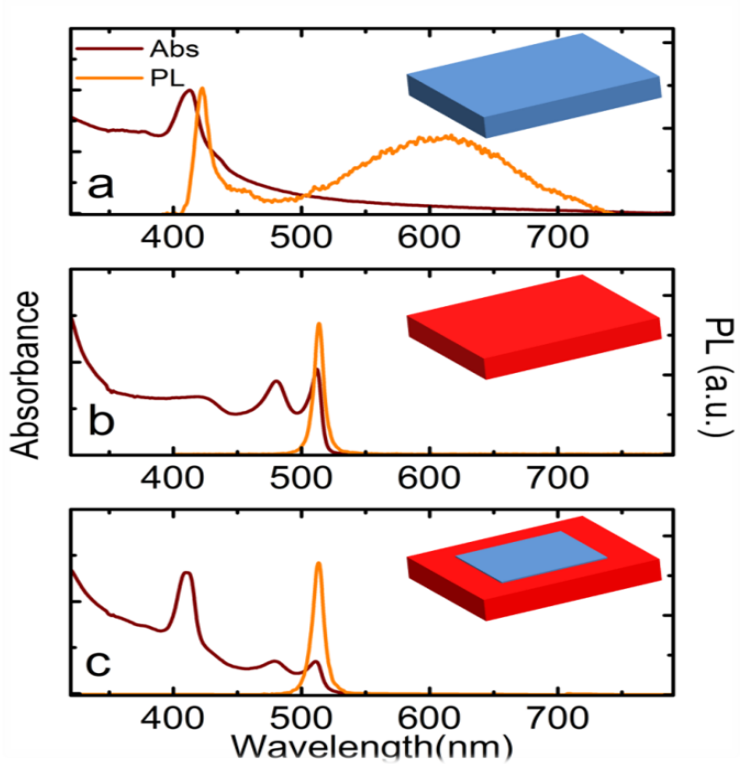

Figure 3.2: Absorption and photoluminescence spectra of (a) 4 ML CdS NPLs, (b) 4 ML CdSe NPLs, and (c) 4 ML CdS/CdSe core/crown NPLs in hexane.

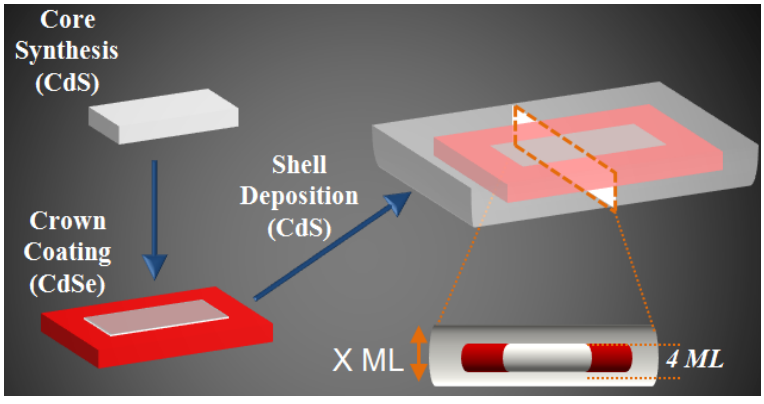

Figure 3.3: A process flow diagram describing the synthesis of QRing structure.

centered at 413 nm [20]. 4 ML CdS NPLs exhibit two photoluminescence peaks, one peak resulting from the band-edge excitonic emission at 421 nm with a full-width-half-maximum (FHWM) value of ∼12 nm and the other one at 613 nm with a FWHM of ∼140 nm resulting from the trap states present in these NPLs (Figure 3.2a). On the other hand, 4 ML-thick CdSe NPLs do not have such trap state emissions (Figure 3.2b). Their photoluminescence spectrum consists of a single peak at 513 nm with a FWHM value of 8.5 nm, which is narrower than that of the CdS NPLs. Also, the light-hole (at 481 nm) and heavy-hole (at 512 nm) transitions of the CdSe NPLs are clearly visible in the absorption spectrum and well separated from each other.

After cleaning, 4 ML CdS NPLs were used as seeds to synthesize CdS/CdSe core/crown hetero-NPLs (see Figure 3.3). The length of the synthesized CdS/CdSe NPLs along the direction they rolled up was measured to be 55 nm 6 nm using (HAADF-TEM) images and these CdS/CdSe NPLs have an emission peak centered at 513 nm, which is similar to that of the 4 ML CdSe NPL cores [65]. This result is a clear indication of the successful CdSe crown coating. Moreover, the presence of sharp excitonic absorption peaks of the both 4 ML CdS and 4 ML CdSe regions (Figure 3.2c) confirms that CdSe was grown only in the lateral direction, not in the vertical direction. The positions of these peaks are 413 nm (∼3.01 eV) for the overlapping CdS light-hole and heavy-hole transitions and 513 nm (∼2.42 eV) for the CdSe heavy-hole transition, which are well correlated with those of the core-only CdS and of the core-only CdSe 4 ML NPLs [20]. As the thickness of NPLs is much smaller than the lateral size of both CdS and CdSe parts, the main quantum confinement results from the vertical thickness of the NPLs and the effect of lateral dimensions on quantum confinement can be ignored. Thus, the existence of the CdS core does not affect the emission spectrum of the CdSe crown to a considerable extent [63]. For the same reason, the position of the sharp absorption peak of the CdS core remains nearly the same and no significant difference in the shape of the peak was observed after the crown coating, as expected. As another observation, the trap-state emission disappears following the CdSe crown coating and a pure, narrow emission spectrum a characteristics of 4 ML CdSe NPLs is attained (Figure 3.2c), as the trap-state

emission results from the defective CdS NPL cores. The complete disappearance of the CdS NPL emission at 421 nm supports the idea that the exciton transfer from the CdS core to the CdSe crown region is very fast and effective. The excitons formed in the CdS cores are transferred to the CdSe crown with the help of fast carrier thermalization/cooling process thanks to the exciton-phonon coupling, valence band offsets, and large exciton binding energy in the order of ∼100 meV [63, 67, 68].

We performed CdS shell deposition on the obtained CdS/CdSe core/crown NPLs to form the QRing heterostructure. The red-shifting absorption peaks of the both CdS core and CdSe crown regions can be seen in Figure 3.4a-b as each shell deposition cycle increases the total thickness of the QRings by 2 ML. Due to the shallow conduction band offset between CdS and CdSe, the electron wavefunction can spread over the CdS shell region and the effective bandgap of the QRings decreases as a result of the diminishing quantum confinement [68]. As another manifestation of the shell coating, the emission peak of the CdSe crown region is shifted towards longer wavelengths after each shell deposition cycle [44]. For the rest of the text, the sample nomenclature for the QRings is given as XSCd, where X is the number of deposition cycles performed on the 4 ML CdS/CdSe core/crown NPLs.

As the CdS/CdSe core/crown cores are the most quantum-confined nanostructures used in this study, the largest red shift occurs after the first shell deposition cycle. The PL peak of the 4 ML CdS/CdSe core/crown NPLs located at 513 nm shifts to 585 nm, corresponding to a red shift of 72 nm (∼297 meV), after 1 cycle of CdS shell deposition. Then, the amount of PL peak shift decreases to 30 nm (∼103 meV), 16 nm (∼51 meV) and finally 12 nm (∼36 meV) for the each succeeding shell deposition cycle. As another observation, the absorption spectrum is dominated by the CdS region as a result of the high atomic ratio of S/Se within the QRings (Figure 3.4c-d), which causes a significant energy difference between the photoluminescence peak and the dominant absorption peak of the QRings. For the 1SCd sample as an example, the ratio of the heavy-hole (at 572 nm) and light-hole (at 538 nm) excitonic absorption peaks of the CdSe crown region to the first absorption peak of the CdS core region (at 457 nm) is found to

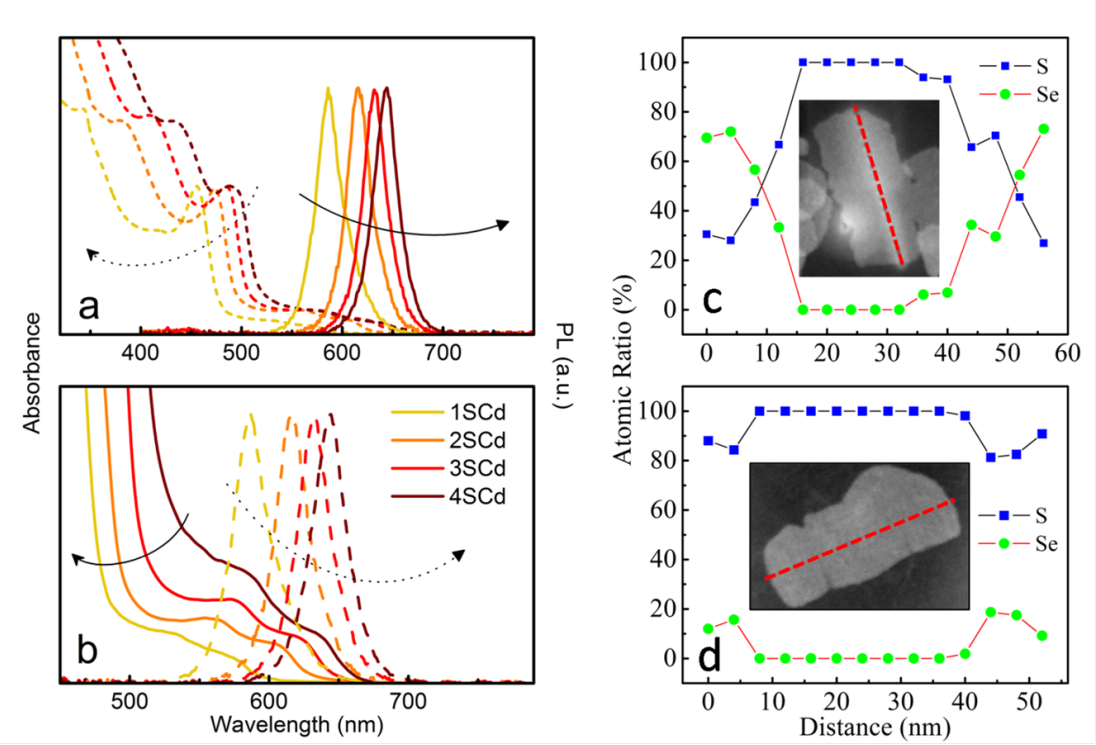

Figure 3.4: (a) Absorption and photoluminescence spectra of CdS/CdSe@CdS QRings, (b) the scaled version of (a) showing the red-shifting absorption peaks of the CdSe crown coated with a varying-thickness CdS shell. (c) EDX Spectrum of 1SCd QRings (inset: TEM image of the respective QRing) and (d) EDX spectrum of 4SCd QRings (inset: TEM image of the respective QRing).

be 44.5 and 19.7 by fitting a multi-component Gaussian curve to the experimental absorption data. The difference in the positions of the first absorption peaks of the CdS core and the CdSe crown is 115 nm, which opens the way for these QRings to be utilized as selective nanoprobes [69–71]. For the case of the sample 4SCd, the ratios reduce to 19.04 and 3.98, respectively; however, the difference in the spectral positions of the first absorption peaks of the CdS core and the CdSe crown exceeds 150 nm.

From Figure 3.1c, we estimated that the average thickness of a monolayer of CdS is ∼0.4 nm within the nanoplatelet structure, which is similar to the value reported in the literature [44]. For example, for 4 cycle CdS coated samples, i.e., the sample 4SCd (4 ML on the upper surface and 4 ML on the lower surface and with 4 ML core size, resulting in 12 ML in total), the total thickness of the nanostructure reaches ∼4.8 nm. As a beneficial side-effect of the shell coating, the folded CdS and the CdS/CdSe NPLs unfold and become flat sheets, as in the case of the only-core small CdSe NPLs, easing the TEM analysis. This observation was previously reported in the literature when shell coating was performed on the folded II-VI NPLs [37].

To support our results on the shell growth, we performed the same shell coating procedure on the CdS NPLs (Figure 3.5). Starting from the as-synthesized 4 ML CdS NPLs, we deposited the CdS shell monolayer by monolayer and observed nearly the same excitonic peaks as in the case for the as-synthesized (4+2X) ML CdS NPLs reported in the literature [20]. The absorption spectra of the 4 ML-core@X ML-shell CdS@CdS NPLs are very similar to those of the 4 ML-core@X ML-shell CdS/CdSe@CdS QRings. However, there are some slight differences between the absorption spectra of the CdS@CdS core@shell NPLs and the CdS/CdSe@CdS core/crown@shell QRings due to the presence of the CdSe crown region in the QRings, in addition to the CdS core region. The absorption spectra of the QRings demonstrate the existence of both the CdS core and the CdSe crown regions and the spectral position of the absorption peaks of the CdS regions is not significantly affected by the presence of the CdSe crown region, for the reason explained before.

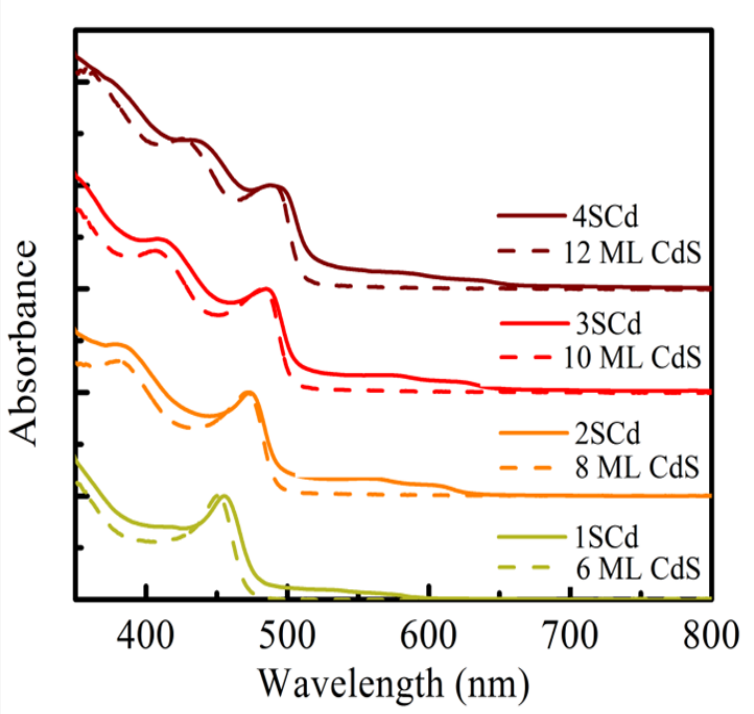

Figure 3.5: Absorption spectra of the core@shell CdS@CdS NPLs (dashed) and CdS/CdSe@CdS QRings (solid).

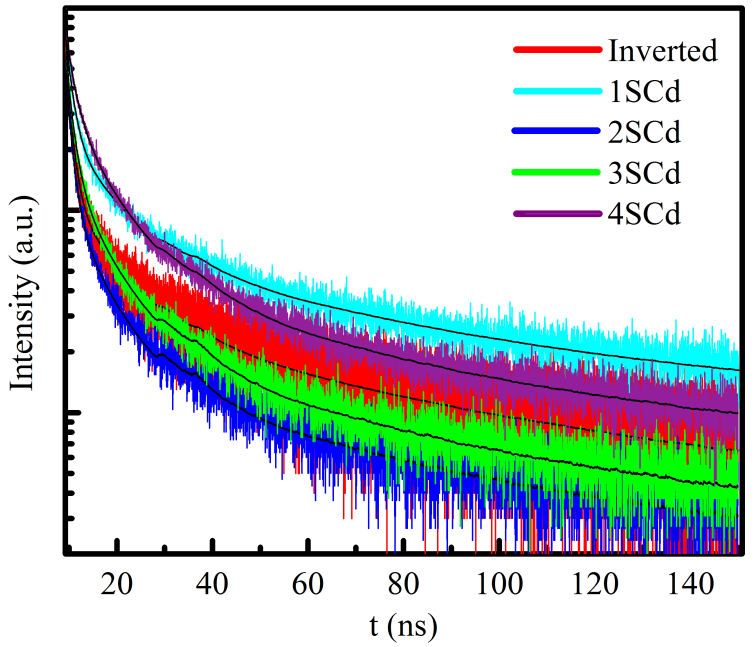

Figure 3.6: TRF curves of the CdS/CdSe core/crown inverted Type-I NPLs (Inverted) measured in hexane and the XSCd QRings (X: 1-4) measured in NMF.

Table 3.1: Lifetime components (in ns), respective fractional contributions (%), and amplitude-averaged lifetime of CdS/CdSe core/crown NPLs (inverted) and of CdS/CdSe@CdS core/crown@shell NPLs (QRings).

Sample	τ_1	τ_2	τ_3	τ_4	$A_1\tau_1$	$A_2\tau_2$	$A_3\tau_3$	$A_4\tau_4$	τ_{AVG}
Inverted	0.15	1.24	9.25	59.37	8.46	17.09	25.65	48.77	1.4
1SCd	0.18	1.34	9.28	58.56	4.16	12.94	29.06	53.82	2.7
2SCd	0.18	1.31	7.53	52.44	16.16	20.73	31.27	31.82	0.9
3SCd	0.21	1.48	7.99	51.38	11.05	20.65	35.55	32.72	1.4
4SCd	0.31	1.91	8.80	51.36	5.21	15.14	41.31	38.31	3.3

From the time-resolved fluorescence decay curves, it can be asserted that the CdS shell coating modifies the emission dynamics of QRings significantly. The fitting of the TRF curves was successfully performed with 4 lifetime components and the fitted curves are given in black lines in Figure 3.6. The respective lifetime components and the amplitude-averaged lifetime of the fitted TRF curves are given in Table 3.1. The amplitude-averaged lifetime of the inverted Type-I CdS/CdSe core/crown NPL cores is found to be ∼1.4 ns (in hexane). After the deposition of the first CdS shell layer, the average lifetime nearly doubles, to 2.7 ns (in NMF). One possible reason behind this prominent change is the lattice strain on the 1 ML-thick CdS shell layer deposited onto each facet of the cores. It has been shown that lattice strain can change material properties dramatically in core/shell colloidal nanocrystals, and it is highly probable that the same effect is in action in our case as well because of the difference in the lattice constants of CdSe and CdS (∼4%) [72]. As the first deposited CdS shell (1 ML on each facet) is thinner than the 4 ML-thick CdSe crown, this crown exerts enough force to the CdS shell to distort its equilibrium lattice, shifting its lattice constant to larger values. This increase in the lattice constant of CdS decreases its bandgap, hence lowering its conduction band level while raising its valence band level. An opposite yet weaker effect is expected in the CdSe crown as it is thicker. This change in the band alignment strengthens the Type-II character of the system and increases the average lifetime significantly. After the deposition of the second CdS shell layer, the force resulting from the lattice mismatch is distributed among the CdS shell layers and the distortion in the first CdS shell layer decreases. As a result, the systems Type-II character becomes weaker than that in the sample

1SCd case and the average lifetime becomes 0.9 ns, shorter than the inverted CdS/CdSe NPLs. Then, a monotonic increase in the average lifetime emanates as the system is now quasi Type-II and the overlap between the electron and hole wavefunctions is reduced with thickening CdS shell. However, it should be noted that the real scenario behind this behavior is more complicated as the QRings are more subject to the environmental effects due to the lack of insulating organic ligands on the surface and there is a significant dielectric constant difference between the polar NMF and the nonpolar hexane solvents. We believe that this may be the reason why the average lifetime of the sample 2SCd is smaller than that of the CdS/CdSe NPLs.

3.4 Conclusion

In summary, we have presented the synthesis and characterization of the CdS/CdSe@CdS QRings having quasi Type-II electronic structure. With suitable growth parameters, nearly pure 4 ML-thick CdS/CdSe core/crown inverted Type-I NPLs were synthesized. After the CdSe crown growth, QRings with a varying-thickness CdS shell were produced via c-ALD procedure. Due to the extension of the carrier wavefunctions, mainly electrons, into the deposited CdS shell layers, the emission and absorption peaks of the QRings red-shift gradually with the deposition of each additional CdS layer. PL quantum yield of these QRings with emission FWHM of $\sim$20 nm was found close to 30%. In addition, an increment in the radiative lifetime was observed, which is a characteristics of reduced oscillator strength in Type-II and quasi Type-II nanostructures. These findings suggest that the QRings are very promising candidates as a model system for bandgap engineering studies and as a possible candidate for use in photonic/optoelectronic applications due to their distinctive optical properties.

Chapter 4

Size-dependent Quantum Yield Enhancement of Aqueous CdTe Quantum Dots Post-treated with Ag^+ Cations

4.1 Introduction

Apart from the general use of nonpolar colloidal quantum dots in the literature, aqueous nanocrystals have a special place in terms of unique applications owing to their functionalized surface and suitability for mass-production. In a typical nonpolar colloidal quantum dots synthesis, the general yield is a few grams at most and it is hard to obtain more nanocrystal with the same quality as the characteristics of the attained nanocrystals changes from batch to batch [73, 74]. Given these, the suitability of aqueous CdTe quantum dots for mass-production plays an important role as the yield of this synthesis can reach tens of grams and can be scaled up further to satisfy the needs [75].

Thanks to the functionalized surface as a result of the aqueous synthesis technique, aqueous nanocrystals do not need extra effort to change the surface ligands as in the case for the nanocrystals synthesized in nonpolar media [76, 77]. They can be directly used in applications including bio-labeling [78, 79], dip-coating [80–82] and magnetic resonance imaging [83,84], which places them among the scientifically interesting and important nanomaterials.

Yet the optical properties of aqueous quantum dots suffer from some problems, including low quantum efficiency. The typical photoluminescence quantum yield of the aqueous CdTe nanocrystals is below 40% in the only-core state and requires additional treatment to achieve higher values. To increase the quantum yield of aqueous CdTe quantum dots, different routes have been shown in the literature including shell coating, surface modification and annealing [85–87]. Among the available options, doping has a special place as it offers an easy and reproducible way to enhance the optical properties of the available nanocrystals. Different variations of doping on aqueous CdTe nanocrystal have been demonstrated and the versatility of the method has been confirmed via experimental data [88–90]. However, these examples have been performed on a limited number of samples and no general information about the behavior of aqueous CdTe quantum dots with different sizes under different doping levels have been understood to date.

In this part of the thesis, we showed that the quantum yield increase with respect to doping level is a strict function of the nanocrystal size and the attainable maximum photoluminescence quantum yield via doping is limited by the choice of the quantum dot size. The quantum yield measurements were supported via time-resolved fluorescence (TRF) measurements and it was shown that the quantum yield increment is due to the increased lifetime of the nanocrystals resulting from the trap state annihilation by dopant atoms. The integrity of the nanocrystal lattice was checked via powder x-ray diffraction (PXRD) measurements and it was confirmed that the CdTe lattice is protected at the doping levels of interest. This work is fully taken from our journal publication article, which is under preparation.

4.2 Experimental Methods

4.2.1 Synthesis of Aqueous CdTe Quantum Dots

The synthesis of aqueous CdTe quantum dots was carried out using a reported method with slight modifications [42]. In a typical synthesis, 4.59 g of $Cd(ClO_4)_2 \cdot 6H_2O$ was dissolved in 500 mL of deionized water in a 3-neck round bottom flask. To this solution, 1.33 g of thioglycolic acid (TGA) was added under constant stirring. The pH of the solution was brought up to 11.8 by the drop-wise addition of 1M NaOH solution. After pH adjustment, the solution was deaerated with bubbling of high-purity argon gas for 30 min. To a separate flask, 0.8 g of Al_2Te_3 was loaded in a glove box as it is an air-sensitive material. Then, this flask was connected to the main flask under argon protection. Subsequently, H_2Te gas was generated via slow addition of H_2SO_4 into the Al_2Te_3-containing flask and the generated gas was carried to main flask with a slow argon gas flow. After the gas generation stopped, argon gas flow was terminated and the main flask was connected to a condenser. The main flask was refluxed at various times to obtain the CdTe quantum dots with different size.

The resulting CdTe QDs were purified via addition of 2-propanol and centrifugation. Finally, they were dissolved in deionized water to obtain 10 μM stock solutions for the doping study.

4.2.2 Ag-Doping of CdTe QDs

For silver doing of CdTe QDs, $AgNO_3$ was dissolved in deionized water to obtain 4 mM solution. Then, a certain amount of this stock solution was added slowly to the vials containing 10 nmol of CdTe QDs (equivalent to1 mL of stock solution) under vigorous stirring.

4.2.3 Absorption, PL and Quantum Yield Measurements

The absorption, photoluminescence, quantum yield, and time-resolved fluorescence measurements were carried out without further purification of the QD dispersions as the purification steps can change both the optical characteristics and the colloidal stability of the cleaned quantum dots.

The quantum yield of the samples was measured by the utilization of the commercial Rhodamine 6G dye dissolved in ethanol as the reference (absolute QY - 0.95). The optical density of the dispersions was kept within the range 0.03-0.05 to ensure the elimination of the self-absorption effects. Then, the absolute quantum yields of the samples were calculated following the method given in Ref. [91].

4.3 Results and Discussion

Aqueous CdTe nanocrystals were synthesized with different size according to the literature method [42]. The normalized photoluminescence and absorption spectra of the resulting nanocrystals are given in Figure 4.1.

For this study, we used 5 different-sized CdTe nanocrystals to show the effect of crystal size on the quantum yield enhancement. The resulting PL peak positions of the nanocrystals are 525, 562, 587, 604 and 621 nm. The full-width-half-maximum (FWHM) values of the PL spectra are larger than those of typical nonpolar CdSe quantum dots, which were 37, 47, 50, 54 and 52nm for S1-5, respectively.

As they are widely utilized in the literature, the properties including extinction coefficients of the core-only CdTe nanocrystals are well known. In this study, the size and concentration of the CdTe nanocrystal dispersions were determined using the experimental size-dependent absorption cross-section provided in [38]. The mathematical formulae describing the size and extinction coefficients of CdTe

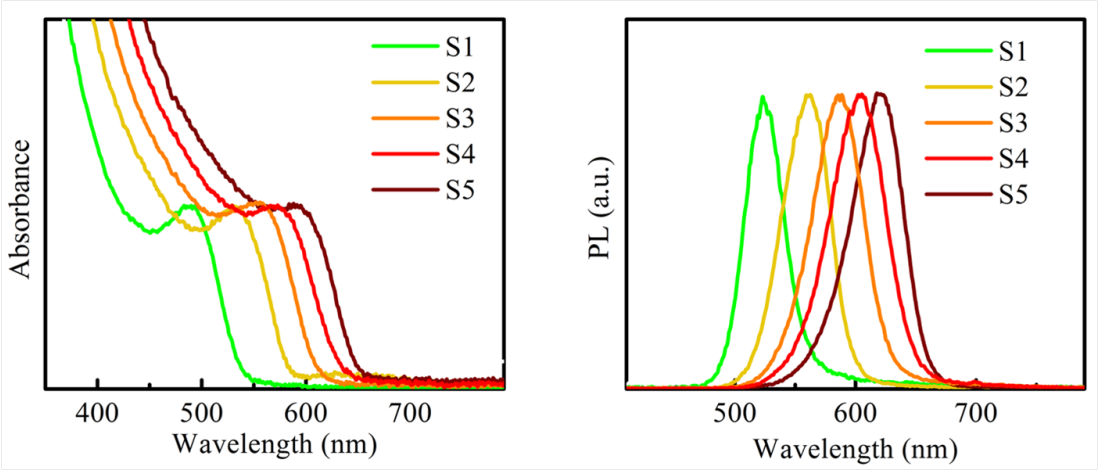

Figure 4.1: Absorption and photoluminescence (PL) spectra of aqueous CdTe quantum dots.

nanocrystals are given in Eq. 4.1.

$$D = 9.8127x10^{-7}\lambda^3 - 1.7174x10^{-3}\lambda^2 + 1.0064\lambda - 194.84 \tag{4.1}$$

$$\epsilon = 10043D^{2.12}$$

Here, λ denotes the position of the first excitonic absorption peak in nanometers, whereas D (nm) gives the size of the quantum dots and ϵ is the extinction coefficient. The calculated size information of our nanocrystals is provided in Table 4.1.

Table 4.1: Size information for 5 different CdTe dispersions used in this study.

Sample	First Absorption Peak (nm)	Photoluminescence Peak (nm)	Size (nm)
S1	489	525	2.01
S2	532	562	3.01
S3	555	587	3.29
S4	572	604	3.44
S5	590	621	3.58

First, we cleaned all the nanocrystal dispersions following the literature method [41]. Then, the stock solutions of each CdTe nanocrystal were prepared by dissolving the CdTe quantum dots in deionized water and the concentration of each

solution was kept fixed at 10 μM. After concentration adjustment, the nanocrystals were placed into glass vials in 1 mL portions, making the amount of nanocrystals in each vial 10 μM x 1 mL = 10 nmol, and treated with Ag^+ ions in solution and the changes in the optical properties were examined through absorption, photoluminescence and time-resolved fluorescence spectroscopy.

From the previous studies, it is a well-known fact that the excess addition of some ions including Ag^+, Hg^{2+} and Cu^{2+} quenches the emission of CdTe/CdSe nanocrystals [92–94]. However, the silver ions in small amounts, generally a few silver ions per nanocrystals, enhance the emission of CdTe nanocrystals [95]. Following these findings, we determined the range in which the addition of silver ions will increase the quantum yield and the experiments were conducted within this range.

To investigate the effect of doping level on optical features, we added increasing amounts of silver ions into the vials and recorded the absorption and emission spectra. With the addition of silver ions, it was observed that the photoluminescence peak of the samples was red-shifted slightly and the quantum yield of the samples increased with varying levels with respect to the amount of the silver ions introduced into the solutions (Figures 4.2-4.3). The reaction takes a few hours to reach completion at most thanks to the fast and effective cation-exchange reaction between Cd^{2+} and Ag^+ ions [96].

A photograph of the S2 series under UV light is given in Figure 4.2. In this figure, the color change of the dispersions is evident, indicating the successful incorporation of the silver ions into the aqueous CdTe nanocrystals.

The red shift observed after the doping process is attributed to the incorporation of the silver ions into the quantum dots, consuming pure CdTe QDs and forming AgCdTe and Ag_2Te QDs. In Figure 4.3, samples belonging to S5 sample set are presented under both day light and UV excitation. As it is clearly seen, the color of the CdTe quantum dots darkens as the doping level increases. If the doping level is increased further, a black-colored dispersion is obtained, indicating the increasing amount of silver telluride.

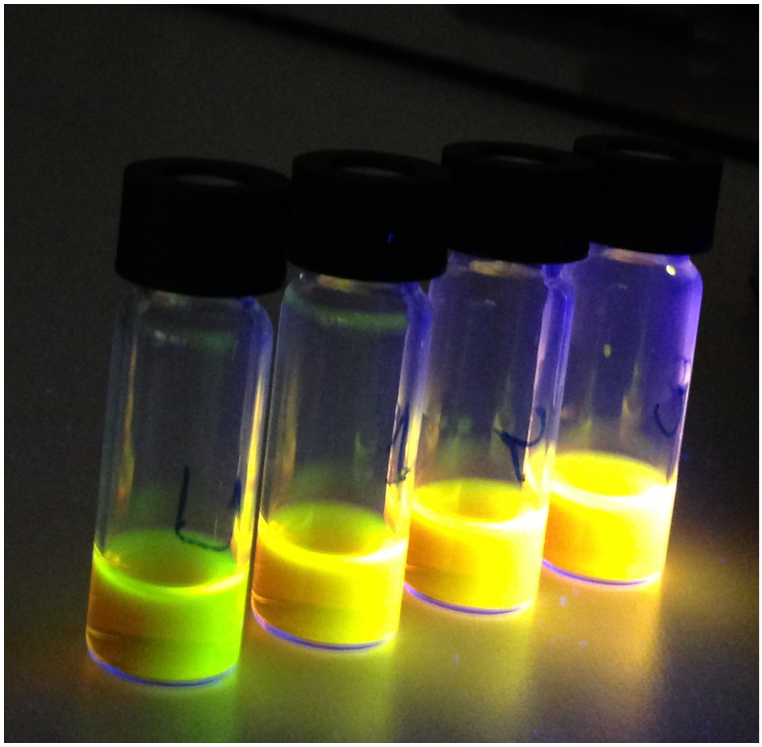

Figure 4.2: S2 series under UV excitation (U: Untreated S2 and 1-3: S2 samples treated with increasing amount of silver ions).

Figure 4.3: S5 series under (left) day light and (right) UV light. The leftmost sample is the cleaned S5 sample without silver addition. The doping level increases towards right. The emission red-shifts and decreases till it disappears as a result of the elevated doping level (The rightmost sample).

To obtain the data presented in Figures 4.4 and 4.5, the absorbance of the nanocrystal dispersions at 468 nm was kept within the 0.03-0.04 range to prevent the self-absorption effects and the absorption value within each sample set was fixed with respect to the undoped sample; thus, the photoluminescence spectra reflect the relative quantum yields of the samples within a sample set. Due to the significant overlapping, the absorption spectra of the sets were given with offset in vertical axis to make the visual inspection of the data easier.

For the small-sized CdTe nanocrystals (Figures 4.4 and 4.6), increase in the quantum yield was apparent and the ratio of the maximum quantum yield obtained to the quantum yield of the stock solution reached ∼2.25 for Sample S1. The absolute quantum yield of Sample S1 went from 10.7% (PL peak ∼525 nm) up to 24.2% (PL peak ∼539 nm), which is a significant number for an aqueous CdTe dispersion at the respective emission peak. Sample S2 had a maximum quantum yield ratio of ∼1.5 with an initial quantum yield of 43% (PL peak ∼562 nm) and a maximum quantum yield of 64% (PL peak ∼573 nm). The values of the initial and maximum QY and the maximum QY ratio for Sample S3 were found to be 38% (PL peak ∼587 nm), 45.7% (PL peak ∼596 nm) and 1.2, respectively.

For the larger CdTe nanocrystals (Figure 4.5), the quantum yield did not increase to a considerable extent. To exemplify, the addition of silver ions did not affect the emission of Sample S5 in a significant way at low doping densities, making the initial quantum yield of the solution (∼50% PL peak ∼621 nm) nearly the same with the doped samples QY (∼49% PL peak ∼625 nm). However, at high doping levels, the photoluminescence of Sample S5 was quenched completely, rendering them useless for photonics/optoelectronics applications (Figure 4.3).

The results presented here can be achieved routinely by applying the procedure given in Section 4.2 - Experimental Methods. However, QDs with even higher quantum efficiency levels can be produced by careful adjustment of the experimental conditions. For example, we could achieve a record high quantum yield of 68% for the doped S2 sample with a very slow addition of 10 μL of silver stock solution and we believe that this value can be pushed up further with careful

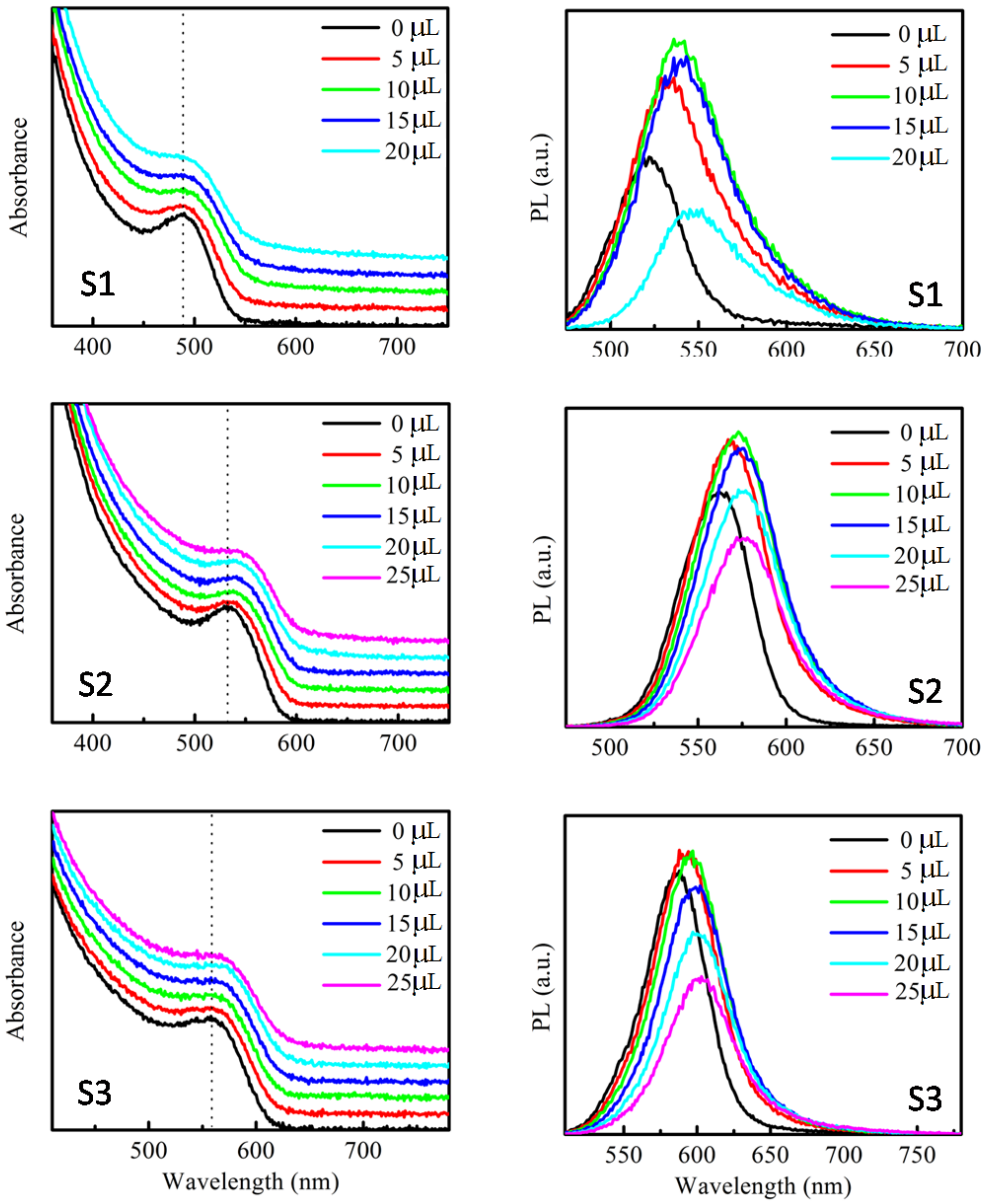

Figure 4.4: Absorption and photoluminescence spectra of aqueous CdTe QDs (S1-3) with different silver cation levels.

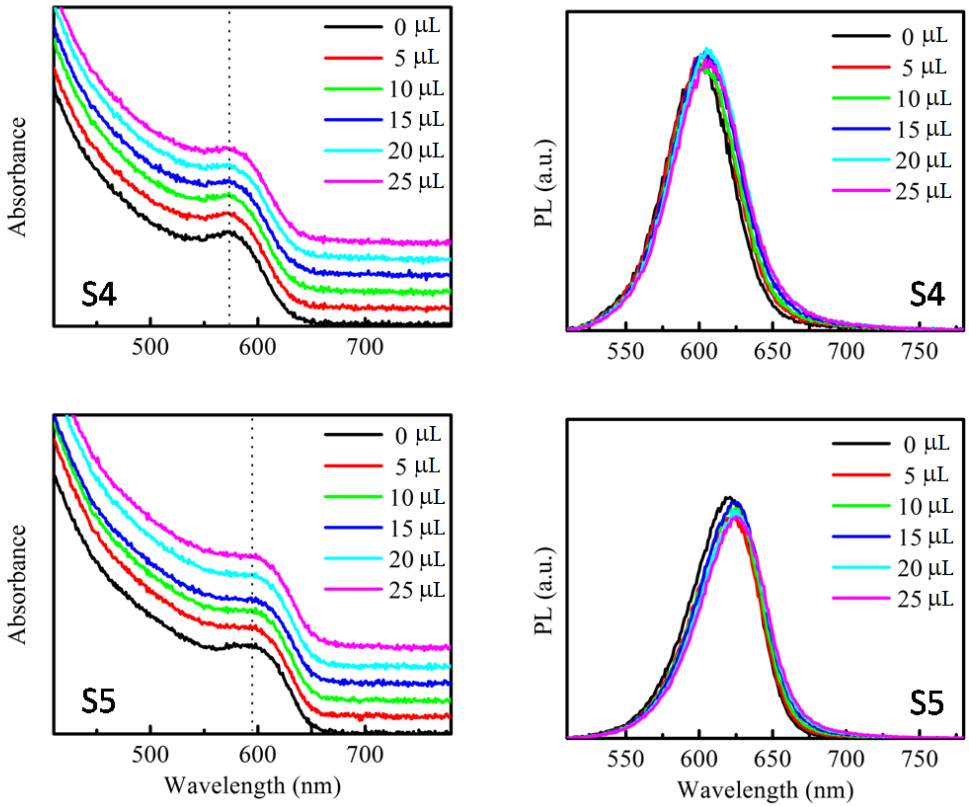

Figure 4.5: Absorption and photoluminescence spectra of aqueous CdTe QDs (S4-5) with different silver cation levels.

adjustment and optimization of the size and doping level.

From the results obtained in this study, the optimal range of silver ions for a successful post-treatment of aqueous CdTe nanocrystals was calculated and it was found to be:

$$\frac{5-15\ \mu\text{L}\ \ \text{x}\ \ 4\ \text{mM}\ \ \text{Ag}^{+}\ \ \text{ions}}{1\ \text{mL}\ \ \text{x}\ \ 10\ \mu\text{M}\ \ \text{nanocrystals}} = 2-6\text{Ag}^{+}\ \ \text{ions/nanocrystal}. \tag{4.2}$$

The calculated amount is similar to the ones reported to be effective in the literature and demonstrates the success of our technique [97]. To gain further deeper insight into the effects of silver ions on CdTe nanocrystals, we performed powder X-ray diffraction (PXRD) study on our samples to observe the differences

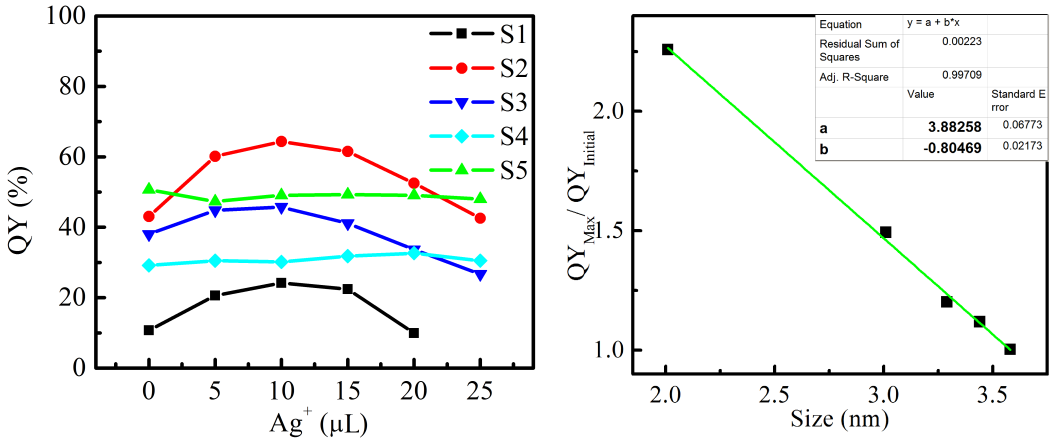

Figure 4.6: Quantum yield of the samples (left) and the maximum relative quantum yield increase with respect to the nanocrystal size.

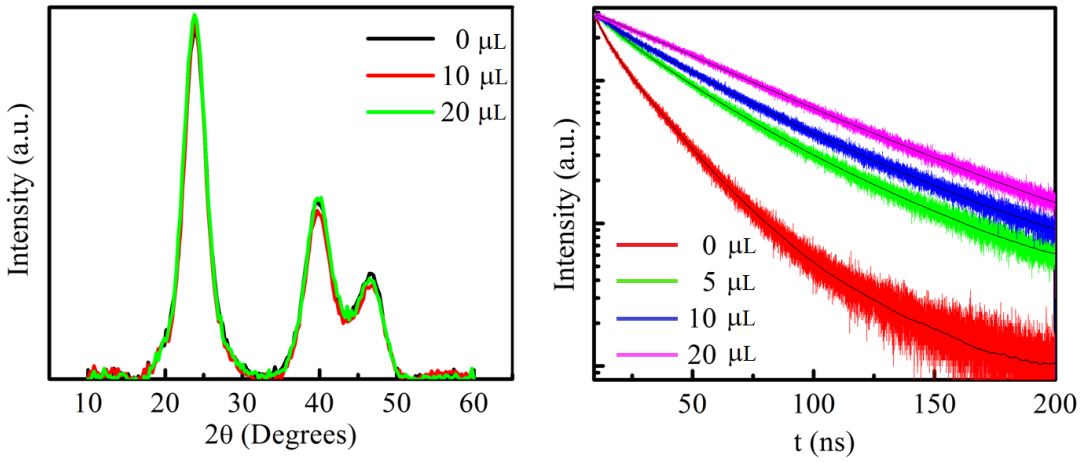

Figure 4.7: (Left) XRD patterns and (Right) TRF curves of CdTe QDs treated with silver ions.

caused by the doping process (Figure 4.7). The samples used for the PXRD study were cleaned multiple times to discard the excess precursor and possible reaction byproducts. Then, the quantum dots were casted into thick films to obtain high enough signal levels. The data presented in Figure 4.7 shows three distinct peaks of CdTe system and confirms the cubic lattice of both the undoped and doped CdTe nanocrystals [78]. As it can be seen, no significant difference among the diffraction curves of the samples exists. Moreover, the PXRD results showed no evidence for the existence of a second phase such as Ag_2Te, confirming the uniform doping of CdTe nanocrystals. This is an expected result since these experiments were carried out at low doping levels and the doping conditions were optimized to obtain uniformly doped nanocrystals.

To find the underlying mechanism behind quantum yield enhancement, time-resolved fluorescence experiments were carried out on these nanocrystals with different levels of doping (Figure 4.7). The nanocrystal dispersions were excited using a pulsed UV laser emitting at 375 nm integrated into the commercial PicoQuant FluoTime 200 TCSPC system. The signal was collected at low excitation density to prevent the interference of higher order kinetics to the results [98].

Table 4.2: Lifetime components (in ns), respective fractional contributions (%), and amplitude-averaged lifetimes of Ag-treated aqueous CdTe dispersions (Sample S2).

Sample	τ_1	τ_2	τ_3	τ_4	$A_1\tau_1$	$A_2\tau_2$	$A_3\tau_3$	$A_4\tau_4$	τ_{AVG}
0 μL	28.53	13.88	3.85	0.70	29.32	47.08	14.84	8.76	15.53
5 μL	44.03	15.99	–	–	67.72	32.28	–	–	34.98
10 μL	49.86	17.48	–	–	78.38	21.62	–	–	42.86
20 μL	56.34	–	–	–	100	–	–	–	56.34

The results demonstrated that the amplitude-averaged lifetime of samples increased significantly by higher levels of silver. The undoped CdTe nanocrystals had an average lifetime of 15.55 ns and the respective TRF decay consisted of 4 lifetime components. Surprisingly, the number of lifetime components decreased by increasing the amount of doping, which indicates the blocking of some exciton decay channels. The blocked channels were found to be the ones with the shortest lifetime values. This indicated that these channels with short lifetimes were

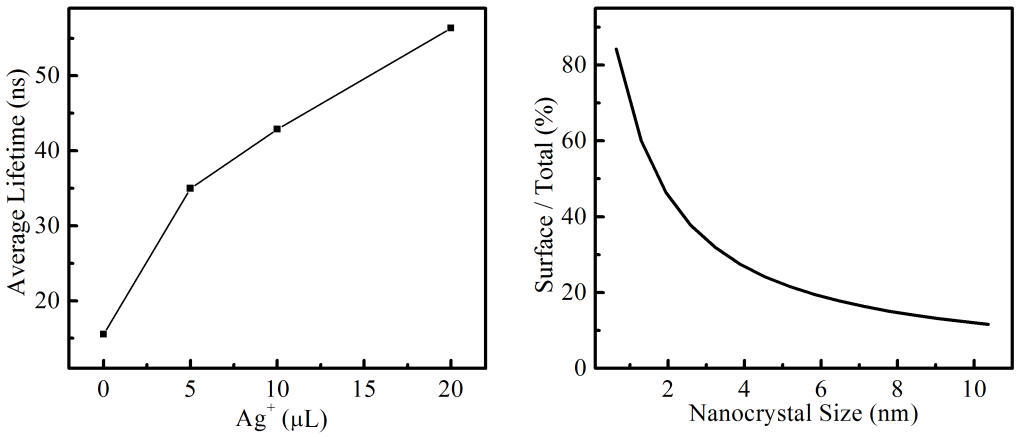

Figure 4.8: (Left) Average lifetime versus the amount of silver ions and (Right) the ratio of the number of the surface atoms to the total number of atoms within a zinc blende CdTe nanocrystal as a function of the nanocrystal size.

related to the nonradiative channels mostly as the suppression of these channels led to an enhancement in quantum yield [42]. In the as-synthesized case, the quantum yield of Sample S2 was measured to be ∼43% and the average lifetime was measured to be 15.53 ns. After addition of 5 μL of silver solution, the quantum yield increased to ∼60%, while the amplitude-averaged lifetime increased to 34.98 ns. When the amount of silver was increased to 10 μL, the average lifetime went up to 42.86 ns. For the 20 μL case, the lifetime became 56.34 ns, which signifies that the relation between the doping level and the lifetime is nonlinear (Figure 4.8).

This trend in lifetime-doping level can be explained by taking the dangling bonds, traps, etc., on the surface of the nanocrystals into consideration. In a recent study, it was shown that the aqueous CdTe QDs have tellurium-related surface traps and that these Te-related traps have a dominant role in low quantum yield of aqueous CdTe nanocrystals via synchrotron X-ray photoelectron spectroscopy measurements [99]. In a later study, the relative energy of these Te-related defects was examined by electrochemical methods and it was concluded that the energy of these traps is around the valence band edge energy of the CdTe quantum dots (Figure 4.9) [100]. Moreover, it was confirmed that the energy of these trap sites is not fixed and changes in accordance with the nanocrystal size.

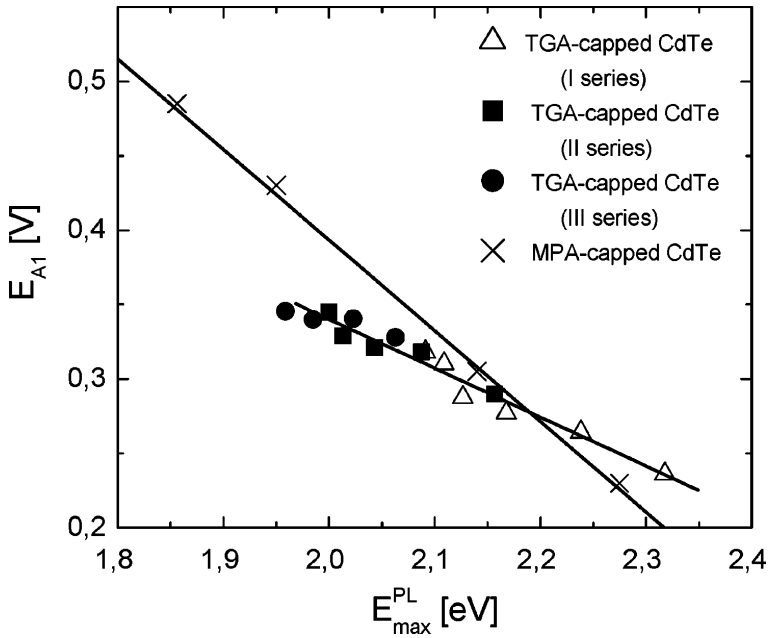

Figure 4.9: Size dependent electrochemical behavior of aqueous CdTe nanocrystals. Reprinted (adapted) with permission from S. K. Poznyak et al. [100] Copyright 2005 American Chemical Society.

For the smaller QDs, these traps sites remain within the bandgap of nanocrystals, facilitating the hole transfer from quantum dots to the Te-defect sites. Thus, these traps cause both the reduced quantum yield and the short average lifetime values. When the size of the nanocrystal is increased, the energy of the traps gets lower while the energy of the valence band edge of the quantum dot gets higher in the energy bandgap diagram [42]. After a certain nanocrystal size, the trap site becomes embedded within the valence band, which makes the hole transfer inefficient (Figure 4.10).

As the surface traps in aqueous CdTe nanocrystals result from the 3-fold coordinated surface Te^{2-} anions, it is expected that Ag^{+} cation can passivate them effectively for it can bind and provide surface Te anions with 4-fold coordination. Furthermore, its ionic radius in +1 oxidation state is similar to that of Cd^{2+} cation, which reduces the possible lattice distortions due to the silver incorporation to the nanocrystals.

Although silver can both undergo cation exchange reaction and attach to the

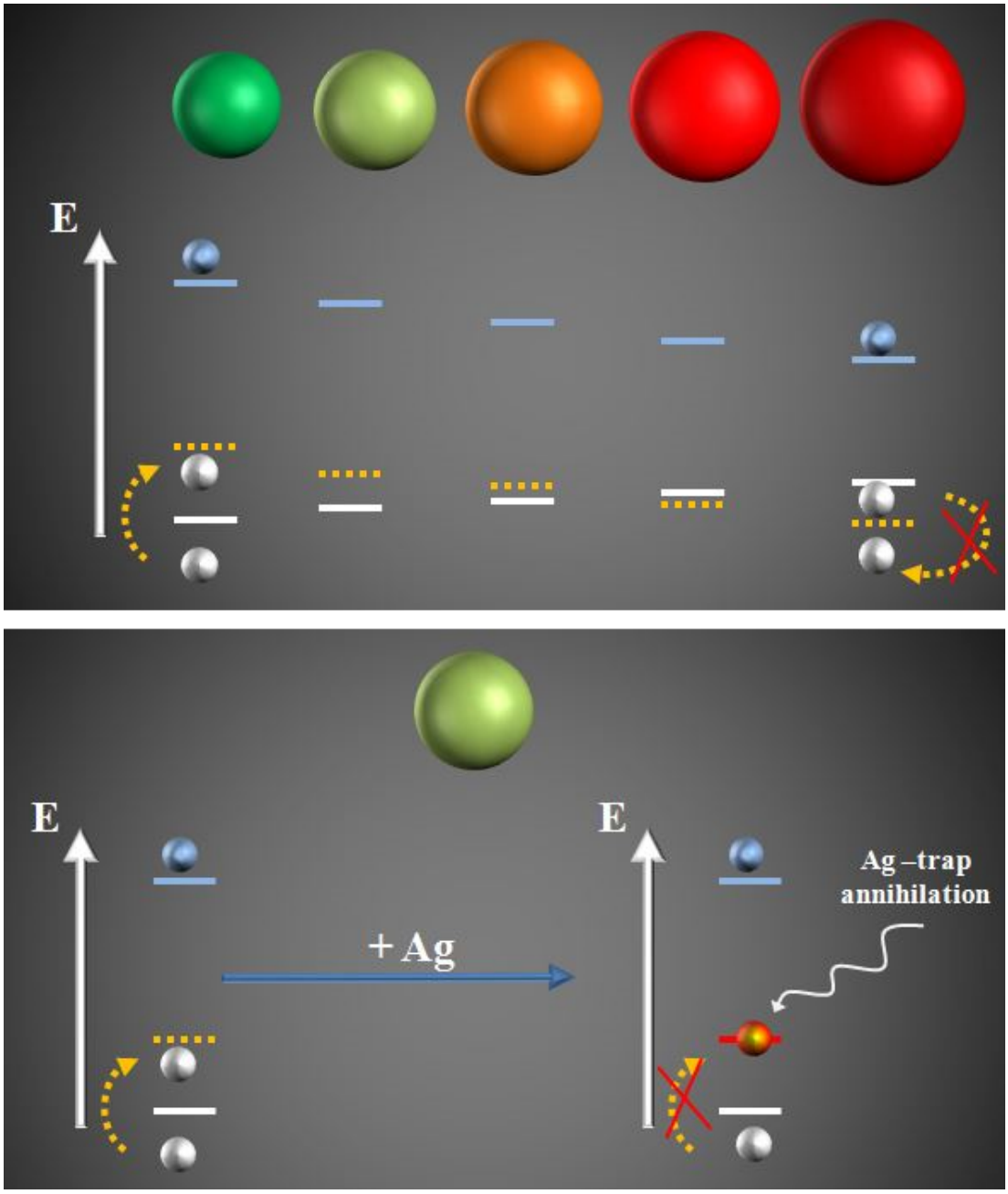

Figure 4.10: (Upper) Size-dependent behavior of the Te-related traps in silver-doped CdTe QDs and (Lower) trap annihilation process by binding of silver atoms to the defect sites. Blue, white and yellow lines represent the positions of conduction and valence band edges and of the Te-related surface traps, respectively.

surface Te atoms, the surface trap annihilation process is more favorable compared to the silver ions replacing the cadmium cations as the surface is more available to such interactions and the replacement of cadmium with silver typically requires more energy. As the as-synthesized quantum dot dispersions have a relatively high density of surface traps, which results from the synthesis procedure and the cleaning steps, the number of silver ions consumed by these surface traps will be higher at the initial stages of doping. With the addition of increasing amount of silver, more of these traps will be annihilated and the number of remaining trap sites will be reduced. After a portion of the surface traps are eliminated, the incorporation of the silver ions into the interior parts of the nanocrystals becomes more favorable. As the silver has a slightly different ionic radius and is in +1 oxidation state, the crystal lattice of the nanocrystals starts to be distorted with increasing number of the replaced cadmium atoms, which results in quantum yield drop.

As another point, by a simple reasoning, the surface-passivating silver atom is expected to behave as an n-type dopant for it binds to the undercoordinated surface Te atom by providing an extra electron. This situation resembles the interstitial doping as in both cases the total number of atoms within the nanocrystal increases. On the other hand, the silver ions replacing cadmium ions within the crystal lattice will assume a p-type doping character due to +1 oxidation state of the silver. From this perspective, it can be concluded that silver enhances the quantum yield if it is introduced as an n-type dopant whereas quenches the emission if it is p-type, which is perfectly consistent with the behavior of the Ag-doped nonpolar CdSe QDs discussed before [97].

Following the surface trap scenario, the size-dependent quantum yield enhancement of CdTe nanocrystals can be explained. In Figure 4.10, the position of the trap sites with respect to the valence band edge is given and the mechanism how silver atoms function to enhance the quantum yield is provided. As the energy of the Te-related surface traps is size-dependent, the effect of silver-doping is also dependent on the nanocrystal diameter. For small QDs, the holes in the valence band of the QDs can be captured by the Te-related surface defects easily. Thus, the quantum efficiency of the QDs can be lowered significantly due to the presence

of such defects. With the addition of a small amount of silver, these defects are eliminated and a huge enhancement in quantum efficiency can be observed. This was ∼2.25-fold for sample S1 in our experiments. When the nanocrystal size gets larger, the Te-related traps become shallower and their quenching effect reduces. As a result, the quantum efficiency recovery ratio reduces as a result of increasing QD size. After the size of QDs exceeds a certain limit, the quantum yield cannot be enhanced via silver doping, for the traps are within the valence band. However, cation exchange reactions can still reduce quantum yield significantly owing to the lattice distortions explained before. The critical size for the as-synthesized core-only MPA-capped CdTe QDs was given ∼4 nm in the literature [42]. For our TGA-capped silver-doped core-only CdTe QDs we found that the critical size is around 3.5 nm.

Moreover, as the number of surface atoms occupies a higher fraction of the total atoms (Figure 4.8) and the effect of surface states on the excitonic dynamics is more pronounced for smaller nanocrystals, it is expected that the recovery of the quantum yield for smaller quantum dots will be greater. This is expected as the carrier wavefunctions of the first excitonic state have the highest probability density at the center of the nanocrystal and the overlap of charge carrier wavefunctions with the surface imperfections is greater for smaller QDs; hence, the charge carriers become more influenced by the surface traps.

The significant change in fluorescence lifetime supports the incorporation of the silver ions into the CdTe nanocrystals. However, to further verify the presence of silver in the Ag-treated CdTe nanocrystals, we used X-ray photoelectron spectroscopy (XPS). As the percentage of silver is minute for our samples presented above ($< 1\%$), new samples with higher doping levels were prepared following the sample preparation steps until a detectable silver signal obtained in the XPS spectra. As we cleaned our samples multiple times to ensure the disposal of the reaction byproducts and unreacted precursor molecules, the signal results only from the silver ions incorporated into the nanocrystals (Figure 4.11). The positions of the cadmium, silver and tellurium peaks are consistent with the XPS spectra of the Ag-doped CdTe quantum dots given in the literature [95].

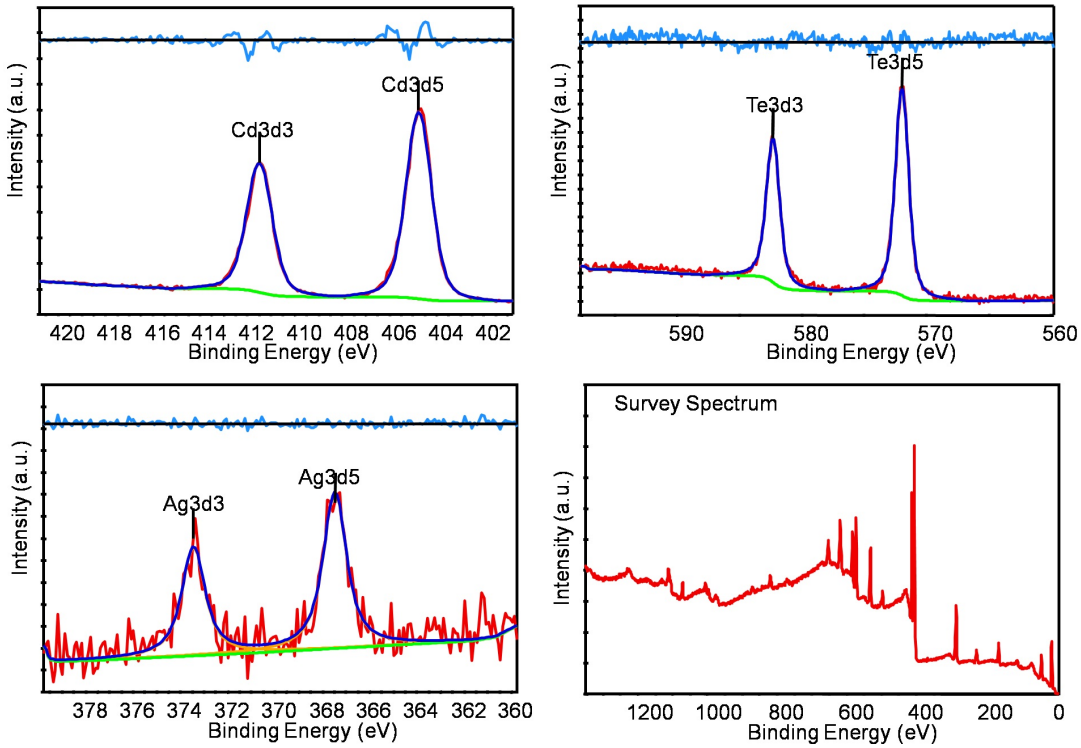

Figure 4.11: XPS analyses of Ag-doped CdTe nanocrystals.

4.4 Conclusion

In this study, we have shown that the quantum yield of the aqueous CdTe quantum dots can be enhanced by utilizing the silver-doping procedure. Via the addition of a suitable amount of silver cations into the quantum dot dispersions, it has been successfully demonstrated that the spectral response of the aqueous CdTe quantum dots can be tuned and the exciton decay kinetics can be changed in a controllable way to obtain nanocrystals with desired properties. Moreover, the mechanism behind the size-dependent quantum yield enhancement for the silver-doped CdTe QDs was explained based on the quantum yield and time-resolved fluorescence measurements. As the last part of the study, the structural integrity of the doped nanocrystals has been confirmed with powder X-ray diffraction measurements and the incorporation of silver into nanocrystals was verified with X-ray photoelectron spectroscopy.

Chapter 5

Colloidal Atomic Layer Deposition-Assisted Doping of CdSe Nanoplatelets

5.1 Introduction

Since the beginning of the nanocrystal research, the doping of the nanocrystals has become a matter of significance as it paves the way for both new and enhanced properties [97]. Among the available elements for the doping of nanoparticles, manganese has a special place thanks to its magnetic properties [61, 101]. The effect of manganese-doping has been explored using nanocrystals belonging to various material systems including II-Se, II-S, II-O and III-V [102–108].

Among these materials, CdSe and CdS nanocrystals have been utilized widely owing to their superior optical performance including high quantum yield, narrow and easily tunable photoluminescence spectrum and availability of different crystal structures and various shapes under ambient conditions. With the introduction of zinc blende CdSe and CdS nanoplatelets, the effect of confinement type on the optical behavior has been shown in various ways, including the distinct

absorption and photoluminescence spectra, higher optical gain coefficients and faster exciton dynamics [65, 109, 110]. Furthermore, the advances in nanoplatelet research have provided us with the capability of controlling the material synthesis and shell-coating with atomic precision via colloidal atomic layer deposition technique (c-ALD) [44].

Although doping of different types of nanomaterials has been shown in the literature, there is no report on the doping of zinc blende CdSe and CdS nanoplatelets. As the thickness of the nanoplatelets reported so far is between 3 and 7 layers of CdSe or CdS, the incorporation of dopant ions into the nanoplatelets presents an overwhelming challenge due to the lattice strain and self-purification system found in nanocrystals [111, 112].

The aim of this study is to demonstrate the eligibility of colloidal atomic layer deposition technique for the successful doping of the zinc blende CdSe@CdS core@shell nanoplatelets. Moreover, c-ALD gives the opportunity to determine the distance of the dopant atoms from the center of NPLs, which enables a novel way to explore the position-dependent behavior of manganese atoms within the resulting NPL nanostructure. This work is partially based on and contains data from our associated journal publication article, which is under preparation.

5.2 Experimental Methods

5.2.1 3 ML CdSe Core Synthesis

First, 217 mg of ($Cd(OAc)_2 \cdot 2H_2O$), 0.3 mmol of Se dissolved in 2 mL of 1-octadecene (ODE), 0.36 mL of oleic acid OA, and 10 mL of ODE were put into a three-neck flask. Under argon protection, the temperature of the flask was raised to 250°C within 20 min and kept at this temperature for 3 min. Then, the flask was quickly cooled down to room temperature. The resulting NPLs were precipitated with the addition of acetone and centrifugation. The supernatant was discarded and the precipitate was dispersed in hexane for further processing.

5.2.2 5 ML CdSe Core Synthesis

5 ML CdSe NPLs were synthesized following a recipe in the literature [20]. 170 mg of cadmium myristate and 14 mL of ODE were put into a three-neck flask and pumped down to remove the air and moisture for 1 h at room temperature. Then, this mixture was heated to 250°C under argon protection. 12 mg of elemental selenium was dissolved in 1 mL of ODE and swiftly injected into this mixture. After one minute, 120 mg of ($Cd(OAc)_2 \cdot 2H_2O$) was added into the flask. The flask was kept at 250°C for 10 min and 0.5 mL of oleic acid was injected before cooling it down to room temperature. CdSe NPLs were precipitated with the addition of acetone and centrifugation. The supernatant was discarded and the precipitate was dispersed in hexane for further processing.

5.2.3 CdS Shell Deposition and Mn-Doping

For the doping study, we used a modified version of the recipe [44]. Mn^{2+} ions were introduced as manganese (II) acetate complex. First, CdSe NPLs were purified to discard the unreacted precursors. After purification, 1 mL hexane solution of CdSe NPLs and 1 mL of NFA were put into a centrifuge tube. Then, aqueous ammonium sulfide was added into this mixture to deposit a sulfur layer onto the NPLs . After the addition, the color of the NPLs changed and the NPLs were transferred to NFA phase. Subsequently, NPLs were seperated out of the reaction mixture by adding toluene–acetonitrile and centrifugation.The supernatant was discarded and the precipitate was dissolved in 1 mL of NFA. The cleaning step was repeated once more to discard the unreacted molecules. Afterwards, the doping was achieved adding $Mn^{2+} - Cd^{2+}$ mixture. This precursor solution was prepared by mixing NFA solutions of manganese (II) acetate and cadmium nitrate tetra hydrate by 1/9 Mn/Cd atomic ratio. The same cleaning procedure was applied to remove the unreacted precursors. Similarly, CdS shell coating was carried out without using manganese (II) acetate solution. As shown in the literature, this step can be repeated as much as needed to achieve the desired NPL shell thickness.

5.3 Results and Discussion

As the first part of this study, we synthesized the CdSe core NPLs with 3 and 5ML thickness (see Figure 5.1). After the purification of the core NPLs, a modified c-ALD procedure was used to introduce the manganese ions into the nanoplatelet structure. As the shell material, we used CdS as it provides nanoplatelets with a quasi Type-II electronic structure, resulting in successful passivation of the CdSe NPL surface [37].

First, the CdSe core NPLs in hexane were sulfur-coated and phase-transferred to n-methyl formamide (NFA) using the aqueous $(NH_4)_2S$ precursor. Then, the NPLs were cleaned and a solution containing nitrate salt of cadmium and the acetate salt of manganese was used for the incorporation of the Mn^{2+} ions. We used the same procedure to obtain the doped versions of the 3 and 5 ML-thick CdSe NPLs. The absorption and PL spectra of the attained Mn-doped CdSe@CdS core@shell NPLs are presented in Figure 5.2.

The presence of the emission tail at the longer wavelength side of the PL spectrum for the doped-NPL with a 3ML CdSe core is significant. Although it seems much like a combination of NPL photoluminescence and manganese emission, we confirmed that the tail resulted from the usage of cadmium nitrate. Our experimental results indicated that the core@shell CdSe@CdS NPLs give a similar PL signal when the cadmium nitrate salt is used even in the absence of the manganese ions, which further confirms that it was not due to manganese ions, but results from the traps formed by cadmium nitrate.

To observe the behavior of this defect state and to determine its characteristics, the c-ALD procedure was repeated on the CdSe@CdS:Mn NPLs without the addition of the $Mn(ace)_2$ into the cadmium precursor solution. After the first cycle of CdS deposition following the manganese doping, the tail emission was decreased; however, its spectral shape did not show any significant change. After the second deposition cycle, the PL spectrum of the doped NPLs became virtually symmetric, indicating the reduced exciton transfer from NPL to the

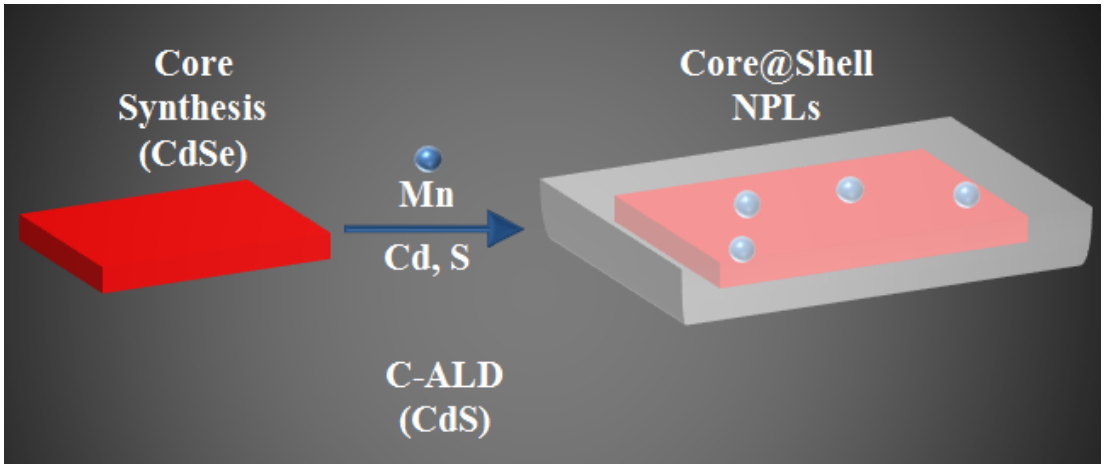

Figure 5.1: A process flow diagram describing the synthesis of Mn-doped NPLs.

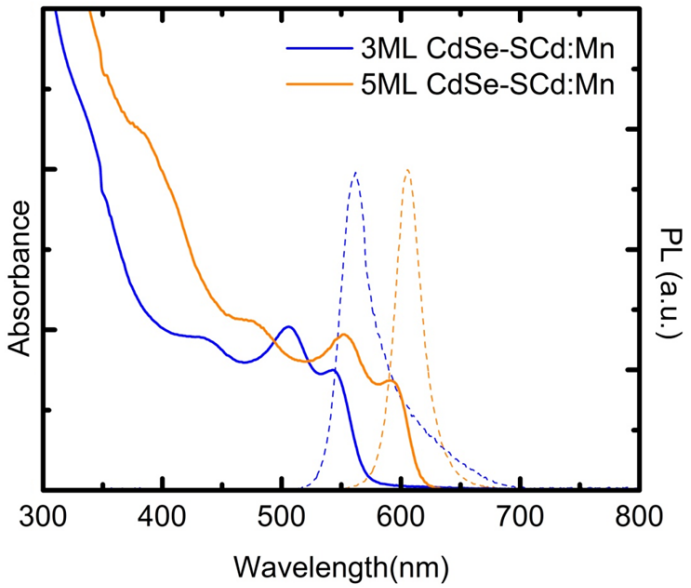

Figure 5.2: Absorption and PL spectra of CdSe@CdS NPLs using 3 and 5 ML-thick CdSe cores.

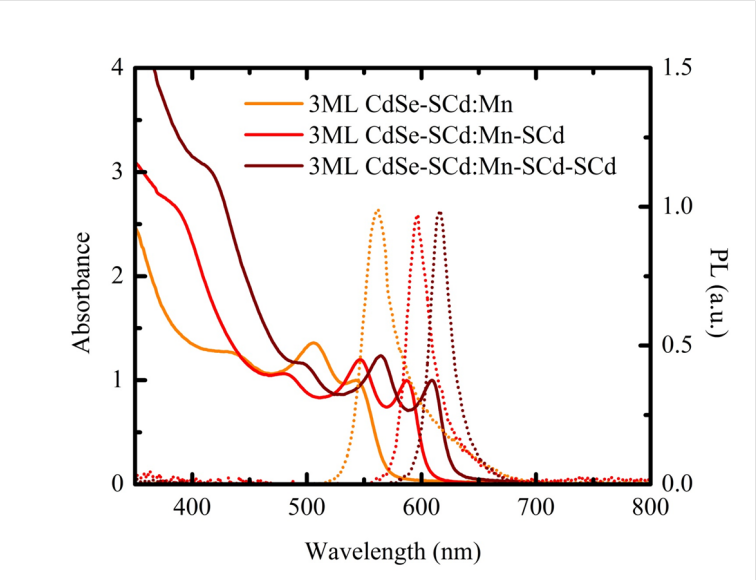

Figure 5.3: Absorption and PL spectra of Mn-doped CdSe@CdS core@shell nanoplatelets with different number of shell layers.

defect states (Figure 5.3). This result suggests that the energy of the trap site is within the bandgap of the doped NPL; however, it goes into either conduction or valence band with weakening quantum confinement. The critical thickness for this transition was found to be (3CdSe + 2SCd:Mn + 4SCd) = 9 ML for our NPLs.

To gain more insight into the exciton dynamics of the resulting NPLs, energy-resolved TRF spectroscopy was utilized (Figure 5.4). Our results indicated a steady increase of the amplitude-averaged lifetime towards lower energy, starting from ∼2 ns at 525 nm up to ∼40 ns at 680 nm, further confirming that the defect emission was not due to the presence of Mn ions as the typical lifetime for Mn dopant emission was reported to be in the order of milliseconds [88]. When combined with the PL spectrum, this shows us that the defect states are long-lived with respect to the band-edge state of the NPLs and their contribution at the low-energy side dominates the PL spectrum of the doped NPLs.

The presence of the manganese within the NPLs was verified via photoluminescence measurements under magnetic field (Figure 5.5). For the magneto-PL measurements, NPLs were excited using the linearly polarized output of a solid

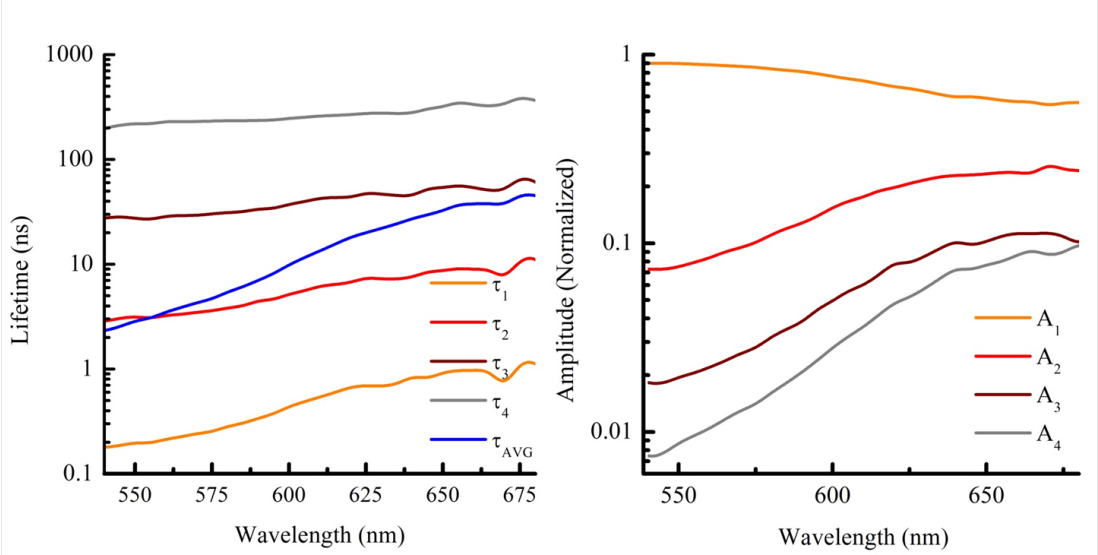

Figure 5.4: Spectral behavior of CdSe@CdS NPLs with 3 ML CdSe core and a Mn-doped CdS shell.

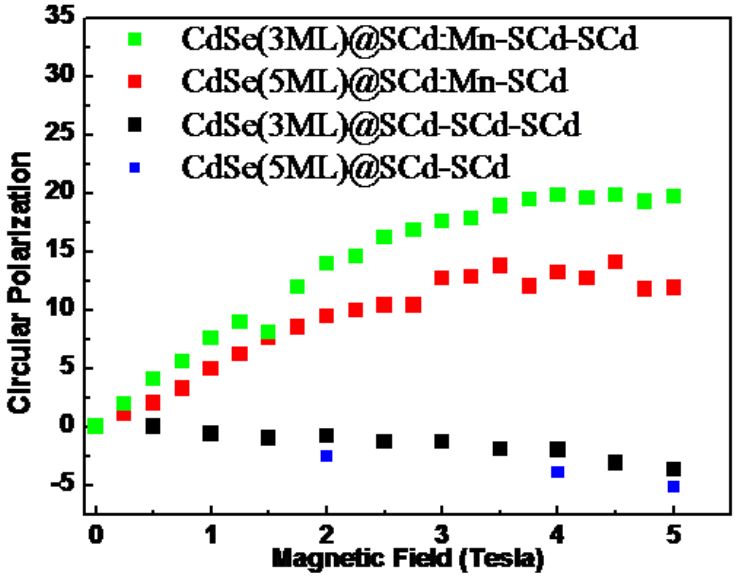

Figure 5.5: Circular polarization of NPL emission under varying magnetic fields at 7 K. (In collaboration with Petrou Lab, Department of Physics, SUNY at Buffalo, Amherst, New York, USA)

state laser emitting at 405 nm and the NPL emission was collected in the Faraday geometry in which applied magnetic field is parallel to direction of the emitted light [113]. The separation of the NPL emission into left and right circularly-polarized components was achieved via a combination of a quarter-wave plate and a linear polarizer. The circular polarization is given by Eq. 5.1.

$$CP = \frac{I_{\sigma^+} - I_{\sigma^-}}{I_{\sigma^+} + I_{\sigma^-}} \tag{5.1}$$

Here, I_{σ^+} and I_{σ^-} are the intensities of the left and right circulary-polarized emission, respectively.

Thanks to the strong magnetic response of manganese, we could measure the magnetic field dependent circular polarization of the doped NPL emission; however, undoped NPLs did not exhibit any significant magneto-optic response under such strong magnetic fields as a result of the intrinsically weak magnetic properties of CdSe and CdS materials. This is a clear indication that manganese is not only incorporated, but it is active within the NPL lattice, as well. Moreover, Figure 5.5 demonstrates that the physical positition of the manganese atoms within NPLs changes the strength of the magnetic response. The doped NPLs with 3 ML CdSe core achieved higher circular polarization than the doped NPLs with 5ML-thick CdSe core could. As the strength of magnetic response is related to the dopant-exciton interaction, the distance of the dopant atoms from the center of the nanoparticles plays a key role. In our method, the manganese ions were placed on the surface of the CdSe cores; however, the distance of the manganese ions to the NPL center for the doped NPLs with 5 ML core is larger than that of the NPLs with 3 ML core by the thichness of a monolayer of CdS. Thus, the spatial overlap of the resulting carrier wavefunctions and dopant atoms is much greater for the doped NPLs with the 3ML cores than that for the ones with the 5 ML core.

5.4 Conclusion

In this study, we have demonstrated the successful doping of zinc blende CdSe NPLs with manganese. The cadmium-nitrate related defect emission and its exciton dynamics were shown via photoluminescence and energy-resolved TRF measurements. The optical behavior of these Mn-doped NPLs was presented under varying magnetic field strengths. The presence and activity of manganese atoms were confirmed by the strong circular polarization of the doped NPLs. Furthermore, the effect of carrier-dopant overlap on the magnetic response strength was demonstrated by placing the manganese atoms in different layers within the NPL structure. It was shown that a greater spatial overlap results in higher magnetic activity for the manganese-doped NPLs.

Chapter 6

Summary and Future Work

In the first part of this thesis work, we showed that the synthesis of complex nanostructures is now possible thanks to the recently introduced nanoplatelet family. Although some simple examples of complex nanostructures were provided in the previous literature, the absence of the nanoplatelet family and the advanced highly anisotropic deposition methods, such as crown coating, has postponed the demonstration of a truly complex nanostructure with profound shape anisotropy. With this thesis study, we demonstrated that such nanostructures can be synthesized using the advanced colloidal deposition methods. Although we have shown only a core/crown@shell nanostructure making a QRing, the same methods can be applied to form more complex structures, enabling the precise bandgap engineering of NPLs to obtain enhanced properties. For the future work, our plan is to demonstrate QRings with continuously tunable emission. The photoluminescence of the NPLs presented in this part can be tuned as shown in the related figures. Also, it is possible to tune the emission of the core/crown NPLs with the adjustment of the lateral size of the CdSe crown. If the lateral size of the crown becomes comparable to the thickness of the NPL, the wavefunction of the carriers will be modified due to the increased quantum confinement. As a result, the effective bandgap of the core/crown NPLs will increase and the emission will blue-shift compared to the core/crown NPLs with large crown sizes. By applying the shell deposition on core/crown NPLs, the continuously tunable emission from

core/crown@shell NPLs will be obtained.

In the second study, we presented a systematic method to probe the internal dynamics of aqueous CdTe QDs when doped with silver atoms. This simple post-processing method has enabled us to explore the size-dependent enhancement of the optical properties of the silver-doped QDs. Our experimental findings indicated that the inconsistencies encountered in the literature on the silver-doped aqueous CdTe QDs may be the result of the nanocrystal size as the response of QDs to silver ions can change significantly with its size. We have found that smaller QDs show a pronounced quantum yield recovery when treated with a suitable amount of silver ions and the increase can easily exceed 2-folds. However, our findings also indicated that the quantum efficiency of the larger QDs cannot be increased via silver treatment. With our experimental data and the earlier findings presented in the literature, we have demonstrated that this results from the existence of under-coordinated tellurium atoms on the surface of the QDs. It was found that silver ions increase the quantum yield of QDs via binding to the surface tellurium atoms, thus making them 4-fold coordinated. Moreover, we discovered that the size-dependent behavior of the silver-doped CdTe QDs is a direct result of the size-dependent position of the surface trap states formed by 3-fold coordinated tellurium atoms. With our systematic study here, it was shown that the critical size for our QDs is around 3.5 nm, which is similar to the value reported in the literature. As a result, we provided a facile way to enhance the optical properties of aqueous CdTe QDs. The future work on this subject will be the investigation of silver doping process on different kinds of nanocrystals. Especially, the ones with lower quantum efficiencies will be examined and a systematic study will be performed to observe the effects of doping. Also, the effects of other ions on the colloidal nanocrystals will be investigated, including both homovalent and heterovalent ions. Among the heterovalent ions for the II-VI family of nanocrystals, +3 ion of manganese has a special place as it can provide nanocrystals with both electronic doping and magnetic properties.

In the third study of this thesis, we proposed and demonstrated a doping method for the zinc blende nanoplatelets for the first time. Our method is based on the colloidal atomic layer deposition technique and proved to be useful for

the doping of nanoparticles with high shape anisotropy. The simplicity and the versatility of the c-ALD process makes it a perfect choice for this kind of doping studies as it is an easy, room-temperature process, and it provides means to control the exact position of the impurity ions. Using the superior position control provided by c-ALD technique, we demonstrated that the exciton-dopant overlap plays a significant role in the determination of the magnetic response. As the carrier wavefunctions of the first state are dense around the center of the NPLs, the exciton-dopant interaction is expected to be stronger if the dopant ion is placed near the center. Indeed, our experimental data showed that the strength of the magnetic response is inversely proportional to the distance of the dopant ions to the center of the NPLs. For our future work, this project will be merged with the QRing project presented previously. With the current method, we can control only the vertical position of the impurities, however the methods used in the QRing project can provide us with alternative methods to control the position of the dopant ions in other directions. Via controlling the position and the amount of manganese ions within the NPLs, we target to increase the circular polarization of the system. As the doped NPLs are still highly emissive, they will be the perfect choice for the realization of the spin-based optoelectronic devices, such as LEDs emitting circularly polarized narrowband light. As another project in this track, the c-ALD assisted doping method will be extended to produce NPLs doped with other ions, such as nickel, magnesium and calcium. With this study we aim to explore the effects of different dopant ions on NPL structures as there is always need for methods to enhance the properties of the available materials. The main goal will be the enhanced quantum yield and less photodegradation, which will enable us to benefit from NPLs as the active material for advanced optoelectronic devices.

To sum up, we have shown the potential and versatility of the nanocrystal synthesis and colloidal post-processing in this thesis work. Via utilization of the proper techniques, nanocrystals with desired properties can be achieved. The simplicity and cheapness of the colloidal synthesis and post-treatment methods combined with the easy-to-perform solution-processing methods developed for

colloidal nanocrystals forms a basis for the utilization of nanocrystals in electronic, photonic and optoelectronic devices. With further advances in this field of research, we believe the nanocrystals will possibly be the material of choice for the production of future large-area devices.

Bibliography

[1] G. H. Wannier, "The Structure of Electronic Excitation Levels in Insulating Crystals," *Phys. Rev.*, vol. 52, pp. 191–197, 1937.

[2] R. J. Elliott, "Intensity of optical absorption by excitons," *Phys. Rev.*, vol. 108, pp. 1384–1389, 1957.

[3] A. P. Alivisatos, "Perspectives on the Physical Chemistry of Semiconductor Nanocrystals," *J. Phys. Chem.*, vol. 100, pp. 13226–13239, 1996.

[4] M. Graf, E. Dupont, H. Luo, S. Haffouz, Z. R. Wasilewski, A. J. S. Thorpe, D. Ban, and H. Liu, "Terahertz quantum well infrared detectors," *Infrared Phys. Technol.*, vol. 52, pp. 289 – 293, 2009.

[5] B. F. Levine, C. G. Bethea, K. G. Glogovsky, J. W. Stayt, and R. E. Leibenguth, "Long-wavelength 128*128 GaAs quantum well infrared photodetector arrays," *Semicond. Sci. Technol.*, vol. 6, p. C114, 1991.

[6] T. Wood, "Multiple quantum well (mqw) waveguide modulators," *J. Light. Technol.*, vol. 6, pp. 743–757, 1988.

[7] S. Nakamura, M. Senoh, S. Nagahama, N. Iwasa, T. Yamada, T. Matsushita, Y. Sugimoto, and H. Kiyoku, "Room–temperature continuous–wave operation of ingan multi–quantum–well structure laser diodes," *Appl.Phys. Lett.*, vol. 69, pp. 4056–4058, 1996.

[8] L. Protesescu, S. Yakunin, M. I. Bodnarchuk, F. Krieg, R. Caputo, C. H. Hendon, R. X. Yang, A. Walsh, and M. V. Kovalenko, "Nanocrystals of

cesium lead halide perovskites ($CsPbX3, X = Cl, Br,$ and I): Novel optoelectronic materials showing bright emission with wide color gamut," *Nano Lett.*, vol. 15, pp. 3692–3696, 2015.

[9] W. Li, R. Zamani, M. Ibez, D. Cadavid, A. Shavel, J. R. Morante, J. Arbiol, and A. Cabot, "Metal ions to control the morphology of semiconductor nanoparticles: Copper selenide nanocubes," *J. Am. Chem. Soc.*, vol. 135, pp. 4664–4667, 2013.

[10] W.-k. Koh, S. R. Saudari, A. T. Fafarman, C. R. Kagan, and C. B. Murray, "Thiocyanate-capped PbS nanocubes: Ambipolar transport enables quantum dot based circuits on a flexible substrate," *Nano Lett.*, vol. 11, pp. 4764–4767, 2011.

[11] S. Sapra, J. Poppe, and A. Eychmuller, "CdSe nanorod synthesis: A new approach," *Small*, vol. 3, pp. 1886–1888, 2007.

[12] S. Deka, A. Quarta, M. G. Lupo, A. Falqui, S. Boninelli, C. Giannini, G. Morello, M. De Giorgi, G. Lanzani, C. Spinella, R. Cingolani, T. Pellegrino, and L. Manna, "CdSe/CdS/ZnS double shell nanorods with high photoluminescence efficiency and their exploitation as biolabeling probes," *J. Am. Chem. Soc.*, vol. 131, pp. 2948–2958, 2009.

[13] P. D. Cozzoli, E. Snoeck, M. A. Garcia, C. Giannini, A. Guagliardi, A. Cervellino, F. Gozzo, A. Hernando, K. Achterhold, N. Ciobanu, F. G. Parak, R. Cingolani, and L. Manna, "Colloidal synthesis and characterization of tetrapod-shaped magnetic nanocrystals," *Nano Lett.*, vol. 6, pp. 1966–1972, 2006.

[14] D. Tar, M. De Giorgi, F. D. Sala, L. Carbone, R. Krahne, L. Manna, R. Cingolani, S. Kudera, and W. J. Parak, "Optical properties of tetrapod-shaped CdTe nanocrystals," *Appl. Phys. Lett.*, vol. 87, p. 224101, 2005.

[15] L. Manna, D. J. Milliron, A. Meisel, E. C. Scher, and A. P. Alivisatos, "Controlled growth of tetrapod-branched inorganic nanocrystals," *Nat. Mater.*, vol. 2, pp. 382–385, 2003.

[16] Q. Pang, Y. Cai, D. P. Nguyen, N. Regnault, N. Wang, S. Yang, W. Ge, R. Ferreira, G. Bastard, and J. Wang, "CdSe Nano-tetrapods: Controllable Synthesis, Structure Analysis, and Electronic and Optical Properties," *Chem. Mater.*, vol. 17, pp. 5263–5267, 2005.

[17] D. D. Vaughn II, D. Sun, S. M. Levin, A. J. Biacchi, T. S. Mayer, and R. E. Schaak, "Colloidal synthesis and electrical properties of GeSe nanobelts," *Chem. Mater.*, vol. 24, pp. 3643–3649, 2012.

[18] R. Costi, G. Cohen, A. Salant, E. Rabani, and U. Banin, "Electrostatic Force Microscopy Study of Single Au-CdSe Hybrid Nanodumbbells : Evidence for Light-Induced Charge Separation," *Nano Lett.*, vol. 9, pp. 2013–2039, 2009.

[19] C. Mondal, A. H. Khan, B. Das, S. Acharya, and S. Sengupta, "Origin of chains of Au-PbS nano-dumbbells in space," *Sci. Rep.*, vol. 3, p. 2612, 2013.

[20] S. Ithurria, M. D. Tessier, B. Mahler, R. P. S. M. Lobo, B. Dubertret, and A. L. Efros, "Colloidal nanoplatelets with two-dimensional electronic structure," *Nat. Mater.*, vol. 10, pp. 936–941, 2011.

[21] V. I. Klimov, A. A. Mikhailovsky, D. W. McBranch, C. A. Leatherdale, and M. G. Bawendi, "Quantization of Multiparticle Auger Rates in Semiconductor Quantum Dots," *Science*, vol. 287, pp. 1011–1013, 2000.

[22] M. Pelton, D. G. Grier, and P. Guyot-Sionnest, "Characterizing quantum-dot blinking using noise power spectra," *Appl. Phys. Lett.*, vol. 85, pp. 819–821, 2004.

[23] O. Chen, J. Zhao, V. P. Chauhan, J. Cui, C. Wong, D. K. Harris, H. Wei, H.-S. Han, D. Fukumura, R. K. Jain, and M. G. Bawendi, "Compact high-quality CdSe-CdS core-shell nanocrystals with narrow emission linewidths and suppressed blinking," *Nat. Mater.*, vol. 12, pp. 445–451, 2013.

[24] B. O. Dabbousi, J. Rodriguez-Viejo, F. V. Mikulec, J. R. Heine, H. Mattoussi, R. Ober, K. F. Jensen, and M. G. Bawendi, "(CdSe)ZnS core-shell quantum dots: Synthesis and characterization of a series of highly luminescent nanocrystallites," *J. Phys. Chem. B*, vol. 101, pp. 9463–9475, 1997.

[25] F. García-Santamaría, Y. Chen, J. Vela, R. D. Schaller, J. A. Hollingsworth, and V. I. Klimov, "Suppressed Auger Recombination in Giant Nanocrystals Boosts Optical Gain Performance," *Nano Lett.*, vol. 9, pp. 3482–3488, 2009.

[26] C. Javaux, B. Mahler, B. Dubertret, A. Shabaev, A. V. Rodina, A. L. Efros, D. R. Yakovlev, F. Liu, M. Bayer, G. Camps, L. Biadala, S. Buil, X. Quelin, and J.-P. Hermier, "Thermal activation of non-radiative Auger recombination in charged colloidal nanocrystals," *Nat. Nanotechnol.*, vol. 8, pp. 206–212, 2013.

[27] Y. Liao, G. Xing, N. Mishra, T. C. Sum, and Y. Chan, "Low threshold, amplified spontaneous emission from core-seeded semiconductor nanotetrapods incorporated into a sol-gel matrix," *Adv. Opt. Mater.*, vol. 24, pp. OP159–164, 2012.

[28] M. Marceddu, M. Saba, F. Quochi, A. Lai, J. Huang, D. V. Talapin, A. Mura, and G. Bongiovanni, "Charged excitons, Auger recombination and optical gain in CdSe/CdS nanocrystals," *Nanotechnology*, vol. 23, p. 015201, 2012.

[29] B. J. Beberwyck and A. P. Alivisatos, "Ion Exchange Synthesis of III - V Nanocrystals," *J. Am. Chem. Soc.*, vol. 134, pp. 19977–19980, 2012.

[30] H. Shao, C. Wang, S. Xu, Y. Jiang, Y. Shao, F. Bo, Z. Wang, and Y. Cui, "Hydrazine-promoted sequential cation exchange: a novel synthesis method for doped ternary semiconductor nanocrystals with tunable emission," *Nanotechnology*, vol. 25, p. 025603, 2014.

[31] J. Park and S.-W. Kim, "CuInS2/ZnS core/shell quantum dots by cation exchange and their blue-shifted photoluminescence," *J. Mater. Chem.*, vol. 21, pp. 3745–3750, 2011.

[32] C. Chen, X. He, L. Gao, and N. Ma, "Cation exchange-based facile aqueous synthesis of small, stable, and nontoxic near-infrared Ag2Te/ZnS core/shell quantum dots emitting in the second biological window," *ACS Appl. Mater. Interfaces*, vol. 5, pp. 1149–1155, 2013.

[33] X. Zhong, Y. Feng, Y. Zhang, Z. Gu, and L. Zou, "A facile route to violet- to orange-emitting Cd x Zn 1- x Se alloy nanocrystals via cation exchange reaction," *Nanotechnology*, vol. 18, p. 385606, 2007.

[34] R. D. Robinson, B. Sadtler, D. O. Demchenko, C. K. Erdonmez, L.-W. Wang, and A. P. Alivisatos, "Spontaneous superlattice formation in nanorods through partial cation exchange," *Science*, vol. 317, pp. 355–358, 2007.

[35] K. A. Abel, P. A. Fitzgerald, T.-y. Wang, T. Z. Regier, M. Raudsepp, S. P. Ringer, G. G. Warr, and F. C. J. M. van Veggel, "Probing the Structure of Colloidal Core / Shell Quantum Dots Formed by Cation Exchange," *J. Phys. Chem. C*, vol. 116, pp. 3968–3978, 2012.

[36] Y. A. Yang, H. Wu, K. R. Williams, and Y. C. Cao, "Synthesis of CdSe and CdTe nanocrystals without precursor injection," *Angew. Chemie*, vol. 44, pp. 6870–6873, 2005.

[37] B. Mahler, B. Nadal, C. Bouet, G. Patriarche, and B. Dubertret, "Core/shell colloidal semiconductor nanoplatelets," *J. Am. Chem. Soc.*, vol. 134, pp. 18591–18598, 2012.

[38] W. W. Yu, L. Qu, W. Guo, and X. Peng, "Experimental Determination of the Extinction Coefficient of CdTe , CdSe , and CdS Nanocrystals," *Chem. Mater.*, vol. 15, pp. 2854–2860, 2003.

[39] R. Xie, U. Kolb, J. Li, T. Basche, and A. Mews, "Synthesis and characterization of highly luminescent CdSe-core CdS/Zn0.5Cd0.5S/ZnS multishell nanocrystals," *J. Am. Chem. Soc.*, vol. 127, pp. 7480–7488, 2005.

[40] W. K. Bae, M. K. Nam, K. Char, and S. Lee, "Gram-Scale One-Pot Synthesis of Highly Luminescent Blue Emitting Cd 1-x Zn x S / ZnS Nanocrystals," *Chem. Mater.*, vol. 20, pp. 5307–5313, 2008.

[41] N. Gaponik, D. V. Talapin, A. L. Rogach, K. Hoppe, E. V. Shevchenko, A. Kornowski, A. Eychmuller, and H. Weller, "Thiol-Capping of CdTe Nanocrystals : An Alternative to Organometallic Synthetic Routes," *J. Phys. Chem. B*, vol. 106, pp. 7177–7185, 2002.

[42] A. L. Rogach, T. Franzl, T. A. Klar, J. Feldmann, N. Gaponik, V. Lesnyak, A. Shavel, A. Eychmuller, Y. P. Rakovich, and J. F. Donegan, "Aqueous synthesis of thiol-capped cdte nanocrystals: State-of-the-art," *J. Phys. Chem. C*, vol. 111, pp. 14628–14637, 2007.

[43] Z. Gu, L. Zou, Z. Fang, W. Zhu, and X. Zhong, "One-pot synthesis of highly luminescent CdTe/CdS core/shell nanocrystals in aqueous phase," *Nanotechnology*, vol. 19, p. 135604, 2008.

[44] S. Ithurria and D. V. Talapin, "Colloidal atomic layer deposition (c-ALD) using self-limiting reactions at nanocrystal surface coupled to phase transfer between polar and nonpolar media," *J. Am. Chem. Soc.*, vol. 134, pp. 18585–18590, 2012.

[45] A. Nag, M. V. Kovalenko, J.-s. Lee, W. Liu, B. Spokoyny, and D. V. Talapin, "Metal-free Inorganic Ligands for Colloidal Nanocrystals : S 2- , HS - , Se 2-, HSe -, Te 2-, HTe -, TeS3 2-, OH -, and NH2 - as Surface Ligands," *J. Am. Chem. Soc.*, vol. 133, pp. 10612–10620, 2011.

[46] P. O. Anikeeva, J. E. Halpert, M. G. Bawendi, and V. Bulovic, "Quantum dot light-emitting devices with electroluminescence tunable over the entire visible spectrum," *Nano Lett.*, vol. 9, pp. 2532–2536, 2009.

[47] C. Dang, J. Lee, C. Breen, J. S. Steckel, S. Coe-Sullivan, and A. Nurmikko, "Red, green and blue lasing enabled by single-exciton gain in colloidal quantum dot films," *Nat. Nanotechnol.*, vol. 7, pp. 335–339, 2012.

[48] G. Konstantatos, I. Howard, A. Fischer, S. Hoogland, J. Clifford, E. Klem, L. Levina, and E. H. Sargent, "Ultrasensitive solution-cast quantum dot photodetectors," *Nature*, vol. 442, pp. 180–183, 2006.

[49] A. G. Pattantyus-Abraham, I. J. Kramer, A. R. Barkhouse, X. Wang, G. Konstantatos, R. Debnath, L. Levina, I. Raabe, M. K. Nazeeruddin, M. Gratzel, and E. H. Sargent, "Depleted-heterojunction colloidal quantum dot solar cells," *ACS Nano*, vol. 4, pp. 3374–3380, 2010.

[50] A. R. Kortan, R. Hull, R. L. Opila, M. G. Bawendi, M. L. Steigerwald, P. J. Carroll, and L. E. Brus, "Nucleation and Growth of CdSe on ZnS Quantum Crystallite Seeds , and Vice Versa , in Inverse Micelle Media," *J. Am. Chem. Soc.*, vol. 112, pp. 1327–1332, 1990.

[51] C. B. Murray, D. J. Norris, and M. G. Bawendi, "Sythesis and Characterization of Nearly Monodisperse CdE (E = S, Se, Te) Semiconductor Nanocrystallites," *J. Am. Chem. Soc.*, vol. 115, pp. 8706–8715, 1993.

[52] X. Peng, L. Manna, W. Yang, J. Wickham, E. Scher, A. Kadavanich, and A. P. Alivisatos, "Shape control of CdSe nanocrystals," *Nature*, vol. 404, pp. 59–61, 2000.

[53] K. P. Rice, A. E. Saunders, and M. P. Stoykovich, "Seed-Mediated Growth of Shape-Controlled Wurtzite CdSe Nanocrystals: Platelets, Cubes, and Rods," *J. Am. Chem. Soc.*, vol. 135, pp. 6669–6676, 2013.

[54] L. Manna, E. C. Scher, and A. P. Alivisatos, "Synthesis of Soluble and Processable Rod- , Arrow- , Teardrop- , and Tetrapod-Shaped CdSe Nanocrystals," *J. Am. Chem. Soc.*, vol. 122, pp. 12700–12706, 2000.

[55] S. Ithurria and B. Dubertret, "Quasi 2D colloidal CdSe platelets with thicknesses controlled at the atomic level," *J. Am. Chem. Soc.*, vol. 130, pp. 16504–16505, 2008.

[56] M. A. Hines and P. Guyot-sionnest, "Synthesis and Characterization of Strongly Luminescing ZnS-Capped CdSe Nanocrystals," *J. Phys. Chem.*, vol. 100, pp. 468–471, 1996.

[57] X. Peng, M. C. Schlamp, A. V. Kadavanich, and A. P. Alivisatos, "Epitaxial Growth of Highly Luminescent CdSe/CdS Core/Shell Nanocrystals with Photostability and Electronic Accessibility," *J. Am. Chem. Soc.*, vol. 119, pp. 7019–7029, 1997.

[58] Z. Chen, B. Nadal, B. Mahler, H. Aubin, and B. Dubertret, "Quasi-2D Colloidal Semiconductor Nanoplatelets for Narrow Electroluminescence," *Adv. Funct. Mater.*, vol. 24, pp. 295–302, 2014.

[59] J. Q. Grim, S. Christodoulou, F. Di Stasio, R. Krahne, R. Cingolani, L. Manna, and I. Moreels, "Continuous-wave biexciton lasing at room temperature using solution-processed quantum wells," *Nat. Nanotechnol.*, vol. 9, pp. 891–895, 2014.

[60] B. Guzelturk, Y. Kelestemur, M. Z. Akgul, V. K. Sharma, and H. V. Demir, "Ultralow Threshold One-Photon- and Two-Photon-Pumped Optical Gain Media of Blue-Emitting Colloidal Quantum Dot Films," *J. Phys. Chem. Lett.*, vol. 5, pp. 2214–2218, 2014.

[61] V. K. Sharma, S. Gokyar, Y. Kelestemur, T. Erdem, E. Unal, and H. V. Demir, "Manganese doped fluorescent paramagnetic nanocrystals for dual-modal imaging," *Small*, vol. 10, pp. 4961–4966, 2014.

[62] J. K. Jaiswal, H. Mattoussi, J. M. Mauro, and S. M. Simon, "Long-term multiple color imaging of live cells using quantum dot bioconjugates," *Nat. Biotechnol.*, vol. 21, pp. 47–51, 2003.

[63] M. D. Tessier, P. Spinicelli, D. Dupont, G. Patriarche, S. Ithurria, and B. Dubertret, "Efficient Exciton Concentrators Built from Colloidal Core/Crown CdSe/CdS Semiconductor Nanoplatelets," *Nano Lett.*, vol. 14, pp. 207–213, 2014.

[64] Y. Kelestemur, M. Olutas, S. Delikanli, B. Guzelturk, M. Z. Akgul, and H. V. Demir, "Type-II Colloidal Quantum Wells: CdSe/CdTe Core/Crown Heteronanoplatelets," *J. Phys. Chem. C*, vol. 119, pp. 2177–2185, 2015.

[65] M. D. Tessier, B. Mahler, B. Nadal, H. Heuclin, S. Pedetti, and B. Dubertret, "Spectroscopy of Colloidal Semiconductor Core/Shell Nanoplatelets with High Quantum Yield," *Nano Lett.*, vol. 13, pp. 3321–3328, 2013.

[66] Z. Li, H. Qin, D. Guzun, M. Benamara, G. Salamo, and X. Peng, "Uniform thickness and colloidal-stable CdS quantum disks with tunable thickness: Synthesis and properties," *Nano Res.*, vol. 5, pp. 337–351, 2012.

[67] A. J. Nozik, "Spectroscopy and hot electron relaxation dynamics in semiconductor quantum wells and quantum dots," *Annu. Rev. Phys. Chem.*, vol. 52, pp. 193–231, 2001.

[68] A. Pandey and P. Guyot-Sionnest, "Intraband spectroscopy and band offsets of colloidal II-VI core/shell structures," *J. Chem. Phys.*, vol. 127, p. 104710, 2007.

[69] Y.-p. Ho, M. C. Kung, S. Yang, and T.-h. Wang, "Multiplexed Hybridization Detection with Multicolor Colocalization of Quantum Dot Nanoprobes," *Nano Lett.*, vol. 5, pp. 1693–1697, 2005.

[70] H.-Y. Yeh, M. V. Yates, A. Mulchandani, and W. Chen, "Molecular beacon-quantum dot-Au nanoparticle hybrid nanoprobes for visualizing virus replication in living cells," *Chem. Commun.*, vol. 46, pp. 3914–3916, 2010.

[71] M. T. Fernandez-Arguelles, A. Yakovlev, R. A. Sperling, C. Luccardini, S. Gaillard, A. S. Medel, J.-M. Mallet, J.-C. Brochon, A. Feltz, M. Oheim, and W. J. Parak, "Synthesis and Characterization of Polymer-Coated Quantum Dots with Integrated Acceptor Dyes as FRET-based nanoprobes," *Nano Lett.*, vol. 7, pp. 2613–2617, 2007.

[72] A. M. Smith, A. M. Mohs, and S. Nie, "Tuning the optical and electronic properties of colloidal nanocrystals by lattice strain," *Nat. Nanotechnol.*, vol. 4, pp. 56–63, 2009.

[73] J.-H. Liu, J.-B. Fan, Z. Gu, J. Cui, X.-B. Xu, Z.-W. Liang, S.-L. Luo, and M.-Q. Zhu, "Green chemistry for large-scale synthesis of semiconductor quantum dots," *Langmuir*, vol. 24, pp. 5241–5244, 2008.

[74] W. K. Bae, K. Char, H. Hur, and S. Lee, "Single-step synthesis of quantum dots with chemical composition gradients," *Chem. Mater.*, vol. 20, pp. 531–539, 2008.

[75] L. Zhou, C. Gao, X. Hu, and W. Xu, "One-pot large-scale synthesis of robust ultrafine silica-hybridized CdTe quantum dots," *ACS Appl. Mater. Interfaces*, vol. 2, pp. 1211–1219, 2010.

[76] S. F. Wuister, I. Swart, F. van Driel, S. G. Hickey, and C. Donega, "Highly Luminescent Water-Soluble CdTe Quantum Dots," *Nano Lett.*, vol. 3, pp. 503–507, 2003.

[77] F. Dubois, B. Mahler, B. Dubertret, E. Doris, and C. Mioskowski, "A Versatile Strategy for Quantum Dot Ligand Exchange," *J. Am. Chem. Soc.*, vol. 129, pp. 482–483, 2007.

[78] M. Green, H. Harwood, C. Barrowman, P. Rahman, A. Eggeman, F. Festry, P. Dobson, and T. Ng, "A facile route to CdTe nanoparticles and their use in bio-labelling," *J. Mater. Chem.*, vol. 17, pp. 1989–1994, 2007.

[79] Z. Li, K. Wang, W. Tan, J. Li, Z. Fu, C. Ma, H. Li, X. He, and J. Liu, "Immunofluorescent labeling of cancer cells with quantum dots synthesized in aqueous solution," *Anal. Biochem.*, vol. 354, pp. 169–174, 2006.

[80] S. Akhavan, B. Guzelturk, V. K. Sharma, and H. V. Demir, "Large-area semi-transparent light-sensitive nanocrystal skins," *Opt. Express*, vol. 20, pp. 25255–2566, 2012.

[81] T. Franzl, D. S. Koktysh, T. A. Klar, A. L. Rogach, J. Feldmann, and N. Gaponik, "Fast energy transfer in layer-by-layer assembled CdTe nanocrystal bilayers," *Appl. Phys. Lett.*, vol. 84, pp. 2904–2906, 2004.

[82] X. Zhang, C. A. Marocico, M. Lunz, V. A. Gerard, Y. K. Gun'ko, V. Lesnyak, N. Gaponik, A. S. Susha, A. L. Rogach, and A. L. Bradley, "Experimental and Theoretical Investigation of the Distance Dependence of Localized Surface Plasmon Coupled Förster Resonance Energy Transfer," *ACS Nano*, vol. 8, pp. 1273–1283, 2014.

[83] F. Zhang, F. He, X.-W. He, W.-Y. Li, and Y.-K. Zhang, "Aqueous synthesis of highly luminescent surface Mn2+ -doped CdTe quantum dots as a potential multimodal agent," *Luminescence*, vol. 29, pp. 1059–1065, 2014.

[84] F. Zhang, T.-T. Sun, Y. Zhang, Q. Li, C. Chai, L. Lu, W. Shen, J. Yang, X.-W. He, Y.-K. Zhang, and W.-Y. Li, "Facile synthesis of functional gadolinium-doped CdTe quantum dots for tumor-targeted fluorescence and

magnetic resonance dual-modality imaging," *J. Mater. Chem. B*, vol. 2, pp. 7201–7209, 2014.

[85] H. Peng, L. Zhang, C. Soeller, and J. Travas-Sejdic, "Preparation of water-soluble CdTe/CdS core/shell quantum dots with enhanced photostability," *J. Lumin.*, vol. 127, pp. 721–726, 2007.

[86] F. Aldeek, L. Balan, G. Medjahdi, T. Roques-carmes, J.-p. Malval, C. Mustin, J. Ghanbaja, and R. Schneider, "Enhanced Optical Properties of Core / Shell / Shell CdTe / CdS / ZnO Quantum Dots Prepared in Aqueous Solution," *J. Phys. Chem. C*, vol. 113, pp. 19458–19467, 2009.

[87] M. Gao, S. Kirstein, H. Möhwald, A. L. Rogach, A. Kornowski, A. Eychmuller, and H. Weller, "Strongly Photoluminescent CdTe Nanocrystals by Proper Surface Modification," *J. Phys. Chem. B*, vol. 102, pp. 8360–8363, 1998.

[88] V. K. Sharma, B. Guzelturk, T. Erdem, Y. Kelestemur, and H. V. Demir, "Tunable White-Light-Emitting Mn-Doped ZnSe Nanocrystals," *ACS Appl. Mater. Interfaces*, vol. 6, pp. 3654–3660, 2014.

[89] R. Zeng, M. Rutherford, R. Xie, B. Zou, and X. Peng, "Synthesis of highly emissive Mn-Doped ZnSe nanocrystals without pyrophoric reagents," *Chem. Mater.*, vol. 22, pp. 2107–2113, 2010.

[90] B. B. Srivastava, S. Jana, N. S. Karan, S. Paria, N. R. Jana, D. D. Sarma, and N. Pradhan, "Highly luminescent Mn-doped ZnS nanocrystals: Gram-scale synthesis," *J. Phys. Chem. Lett.*, vol. 1, pp. 1454–1458, 2010.

[91] M. Grabolle, M. Spieles, V. Lesnyak, N. Gaponik, A. Eychmuller, and U. Resch-Genger, "Determination of the Fluorescence Quantum Yield of Quantum Dots : Suitable Procedures and Achievable Uncertainties," *Anal. Chem.*, vol. 81, pp. 6285–6294, 2009.

[92] P. P. Ingole, R. M. Abhyankar, B. L. V. Prasad, and S. K. Haram, "Citrate-capped quantum dots of CdSe for the selective photometric detection of silver ions in aqueous solutions," *Mater. Sci. Eng. B*, vol. 168, pp. 60–65, 2010.

[93] C. Wang, J. Zhao, Y. Wang, N. Lou, Q. Ma, and X. Su, "Sensitive Hg (II) ion detection by fluorescent multilayer films fabricated with quantum dots," *Sensors Actuators B*, vol. 139, pp. 476–482, 2009.

[94] M. T. Fernández-Argüelles, J. J. Wei, J. M. Costa-Fernández, R. Pereiro, and A. Sanz-Medel, "Surface-modified CdSe quantum dots for the sensitive and selective determination of Cu(II) in aqueous solutions by luminescent measurements," *Anal. Chim. Acta*, vol. 549, pp. 20–25, 2005.

[95] S.-J. Ding, S. Liang, F. Nan, X.-L. Liu, J.-H. Wang, L. Zhou, X.-F. Yu, Z.-H. Hao, and Q.-Q. Wang, "Synthesis and enhanced fluorescence of Ag doped CdTe semiconductor quantum dots," *Nanoscale*, vol. 7, pp. 1970–1976, 2015.

[96] B. J. Beberwyck, Y. Surendranath, and A. P. Alivisatos, "Cation exchange: A versatile tool for nanomaterials synthesis," *J. Phys. Chem. C*, vol. 117, pp. 19759–19770, 2013.

[97] A. Sahu, M. S. Kang, A. Kompch, C. Notthoff, A. W. Wills, D. Deng, M. Winterer, C. D. Frisbie, and D. J. Norris, "Electronic impurity doping in CdSe nanocrystals," *Nano Lett.*, vol. 12, pp. 2587–2594, 2012.

[98] A. F. Cihan, P. L. Hernandez Martinez, Y. Kelestemur, E. Mutlugun, and H. V. Demir, "Observation of biexcitons in nanocrystal solids in the presence of photocharging," *ACS Nano*, vol. 7, pp. 4799–4809, 2013.

[99] H. Borchert, D. V. Talapin, N. Gaponik, C. McGinley, S. Adam, A. Lobo, T. Möller, and H. Weller, "Relations between the photoluminescence efficiency of CdTe nanocrystals and their surface properties revealed by synchrotron XPS," *J. Phys. Chem. B*, vol. 107, pp. 9662–9668, 2003.

[100] S. K. Poznyak, N. P. Osipovich, A. Shavel, D. V. Talapin, M. Gao, A. Eychmuller, and N. Gaponik, "Size-dependent electrochemical behavior of thiol-capped CdTe nanocrystals in aqueous solution," *J. Phys. Chem. B*, vol. 109, pp. 1094–1100, 2005.

[101] S. Wang, B. R. Jarrett, S. M. Kauzlarich, and A. Y. Louie, "Core/Shell Quantum Dot QD w high relaxivity & photoluminescence for multimodality imaging," *J. Am. Chem. Soc.*, vol. 129, pp. 3848–3856, 2007.

[102] Y. Sahoo, P. Poddar, H. Srikanth, D. W. Lucey, and P. N. Prasad, "Chemically fabricated magnetic quantum dots of InP : Mn," *J. Phys. Chem. B*, vol. 109, pp. 15221–15225, 2005.

[103] O. D. Jayakumar, H. G. Salunke, R. M. Kadam, M. Mohapatra, G. Yaswant, and S. K. Kulshreshtha, "Magnetism in Mn-doped ZnO nanoparticles prepared by a co-precipitation method," *Nanotechnology*, vol. 17, pp. 1278–1285, 2006.

[104] N. S. Norberg, K. R. Kittilstved, J. E. Amonette, R. K. Kukkadapu, D. A. Schwartz, and D. R. Gamelin, "Synthesis of Colloidal Mn 2 + : ZnO Quantum Dots and High-T C Ferromagnetic Nanocrystalline Thin Films," *J. Am. Chem. Soc.*, vol. 126, pp. 9387–9398, 2004.

[105] W.-C. Kwak, Y.-M. Sung, T. G. Kim, and W.-S. Chae, "Synthesis of Mn-doped zinc blende CdSe nanocrystals," *Appl. Phys. Lett.*, vol. 90, p. 173111, 2007.

[106] M. Azad Malik, P. O'Brien, and N. Revaprasadu, "Synthesis of TOPO-capped Mn-doped ZnS and CdS quantum dots," *J. Mater. Chem.*, vol. 11, pp. 2382–2386, 2001.

[107] H. F. Wang, Y. He, T. R. Ji, and X. P. Yan, "Surface molecular imprinting on Mn-doped ZnS quantum dots for room-temperature phosphorescence optosensing of pentachlorophenol in water," *Anal. Chem.*, vol. 81, pp. 1615–1621, 2009.

[108] N. Pradhan and X. Peng, "Efficient and color-tunable mn-doped znse nanocrystal emitters: Control of optical performance via greener synthetic chemistry," *J. Am. Chem. Soc.*, vol. 129, pp. 3339–3347, 2007.

[109] J. Huang, M. V. Kovalenko, and D. V. Talapin, "Alkyl chains of surface ligands affect polytypism of cdse nanocrystals and play an important role

in the synthesis of anisotropic nanoheterostructures," *J. Am. Chem. Soc.*, vol. 132, pp. 15866–15868, 2010.

[110] D. V. Talapin, J. H. Nelson, E. V. Shevchenko, S. Aloni, B. Sadtler, and A. P. Alivisatos, "Seeded growth of highly luminescent CdSe/CdS nanoheterostructures with rod and tetrapod morphologies," *Nano Lett.*, vol. 7, pp. 2951–2959, 2007.

[111] G. M. Dalpian and J. R. Chelikowsky, "Self-purification in semiconductor nanocrystals," *Phys. Rev. Lett.*, vol. 96, p. 226802, 2006.

[112] D. J. Norris, A. L. Efros, and S. C. Erwin, "Doped nanocrystals," *Science*, vol. 319, pp. 1776–1779, 2008.

[113] R. Viswanatha, J. M. Pietryga, V. I. Klimov, and S. A. Crooker, "Spin-polarized Mn2+ emission from mn-doped colloidal nanocrystals," *Phys. Rev. Lett.*, vol. 107, p. 067402, 2011.